Node Duplication in Disease Maps using Graph Neural Networks

Benjamin Moser

October 25, 2021

Abstract

Contents

List of Figures

List of Tables

1 Introduction

Overview ...

Problem Statement ...

Motivation for Approach ...

Structure ...

2 Background

2.1 Biological Networks

The behaviour of biological systems is often shaped by complex interactions. The set of entities in a system and their interactions (relationships) naturally form a network. We refer to a biological entity in such an interaction network as *species*. Choices of what species and relationships to consider yield different kinds of biological networks.

Protein-protein interaction (PPI) networks describe the complex interactions between different proteins. Analysing the entire network of interactions is interesting because the effective biological function of proteins is rarely defined based on their identity alone, but rather on their roles as enzymes or signalling molecules in relationship to other proteins. PPI networks can be useful to infer the biological function of an unknown protein or gene, or to group functionally similar proteins.

A *metabolic model* of some organism consists of a formally described set of chemical compounds (*metabolites*) as well as a set of chemical reactions or interactions between the metabolites. Computational analysis methods on metabolic networks can be used to predict the growth of an organism under specific conditions, identify key intervention targets to alter metabolic processes, or identify relatively independent metabolic subsystems.

Disease maps visually describe species and interactions that are of relevance to a specific disease. They serve as a comprehensive and coherent collection of existing knowledge that is otherwise scattered across individual publications.

Species and relationships need not necessarily have a direct physical counterpart. Several works investigate the interactions between diseases, drugs, or phenotypes, potentially connecting concrete physical entities (such as proteins) to abstract entities (such as, for instance, drug side effects) [1, 2]. Moreover, biological networks may serve as a scaffold to put data on individual species into relation with one another.

2.2 Disease Maps

Individual biochemical pathways can be described visually by *process description diagrams*. Species are represented visually as discs or boxes and are linked by lines representing chemical processes. We refer to the visual representation of a species as a *species alias*. Such diagrams have traditionally been used to describe reaction cascades and metabolic subsystems, first in the form of hand-drawn illustrations and later as computer-generated graphics. An example is given in Figure 2.1.

However, several diseases such Alheimer's Disease or Parkinson's Disease do not depend merely on a single mechanism. Rather, they are thought to arise through complex interactions of biological processes or genetic and environmental factors. Knowledge on relevant factors is obtained incrementally and scattered across individual publications or database entries. Thus, a systematic understanding of the involved processes and their relationships is essential [3, 4].

For several diseases, experts have assembled *disease maps*, comprehensive visual diagrams combining all known mechanisms relevant for a given disease. These diagrams are particularly suited for visual, interactive exploration. An example is given in Figure 2.1.

Traditionally, such diagrams have been drawn as pixel- or vector-based graphics. Formalised, digital representations provide several advantages:

- Creating a disease map requires a high amount of effort and domain knowledge. The extraction of knowledge from scientific publications or databases, as well as finding an adequate visual layout can be supported by computational tools.
- Entities in the diagram may be annotated with additional information such as links to research publication or database entries.
- A formalised representation enables the use of computational methods for analysis and interactive exploration (see Related Work).

Although their content is based on biological processes, disease maps differ in nature from other types of biological networks in the following aspects:

- Disease maps are assembled based on the judgement of their curators. Only processes that are deemed relevant or informative to the given objective are included.
- While other biological networks such as PPI networks or metabolic networks are defined mainly by their abstract network structure, a disease map is an actual visual diagram. Species and relationships have been laid out to optimally present the included information.
- Recent disease maps contain up to several thousands of species and reactions and are very rich in information beyond the mere enumeration of species and their pairwise relationships. For example, a disease map may contain different types of species such as proteins, genes, phenotypes *etc.*. Species may have different states (e.g. "phosphorylated") and be nested in *complexes* (groups). Further, species and relationships are often annotated with links to external databases such as Entrez Gene [5] or UniProt [6]. This poses special challenges particularly for layout and interactive exploration.

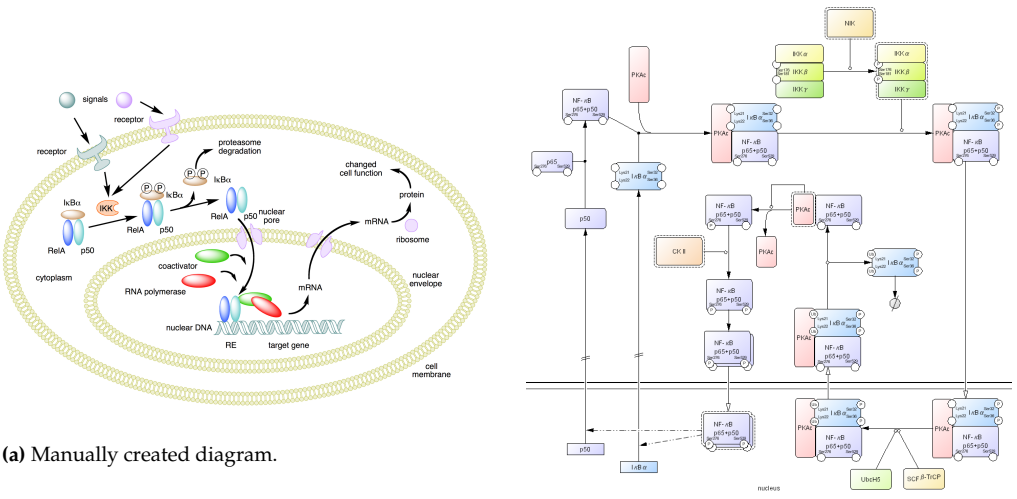

(a) Manually created diagram.

(b) Diagram as created with CellDesigner.

Figure 2.1: Two representations of prototypical mechanisms of NF-κB -signaling.

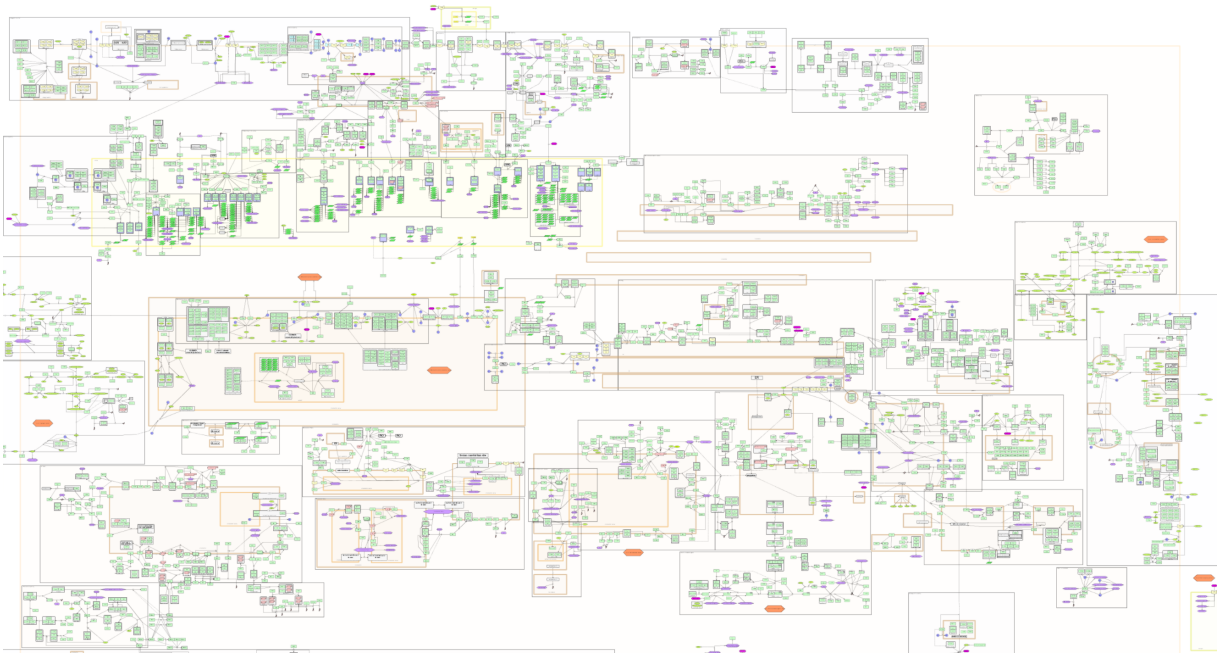

Figure 2.2: Excerpt of PDMAP [7], describing molecular mechanisms of Parkinson's Disease.

2.3 Drawing of Biological Process Diagrams

The most widely used and intuitive visualisation paradigm is the *node-link diagram* in which nodes are represented graphically as dots, circles or boxes and edges are represented by lines. For sake of simplicity, we use *nodes* and *edges* ambiguously both in their mathematical sense and for their graphical representations. Finding a *layout* of a graph (also called *graph drawing*) means finding positions for node representations and potentially also routing edges. What makes a good layout generally depends on the specific kind of network data and the task of the consumer of the visualisation. In general, a good layout is commonly required to avoid edge crossings or overlapping nodes, to be compact and to keep euclidean distances proportional to graph distances. Additional constraints may be for example the preservation of symmetries, clear representation of hierarchical structure or preservation of a viewer's mental map when updating a dynamically changing graph layout. Automatic graph layouting is a highly studied topic and numerous different methods are available (see Section 3).

Biological process diagrams, however, often contain subgraphs with particular semantics, which must be considered explicitly in the layout in order to convey the contained information as effectively as possible. Because of this, it is still common practise to draw such diagrams manually, or to obtain an initial automatic layout and adjust that manually. This process is extremely time-consuming and often requires specific domain knowledge. We outline some of the challanges in drawing biological process diagrams [8, 9, 10]:

- Large diagrams such as the disease maps considered in this work often exhibit a clear structural and visual hierarchy.
- Biochemical reactions often involve main substrates and products as well as secondary cofactors and enzymes. Substrates and products are usually placed orthogonally on opposite sides while cofactors and enzymes are placed on the side.
- Biological pathways often involve reaction cascades. These should be displayed such that the cascade is distuingishable and easy to follow. It may be preferrable to align cascades to the natural reading direction of the viewer (commonly top-to-bottom and left-to-right).
- Some biological pathways involve cyclic patterns and these should be clearly distuingishable as such.
- Biological process description diagrams may contain more information than merely species and reactions. Species can be (recursively) grouped into complexes. A complex is commonly represented as a box containing the visual representation of the species and thus its contents also need to be laid

out. Further, cellular compartments are also commonly represented visually as large boxes or frames containing the biological processes therein. Since transport in and out of the compartment and other reactions involving the membranes are of high biological relevance, proper placement of nodes and edges inside, outside or on the boundary of compartments is critical.
- It may be the case that a single species often is involved in several different biological processes. It may be preferrable to represent that species by multiple, separate visual representations.

The question of if and when to represent a species by multiple different visual representations instead of a single one is exactly the focus of this work.

Node Duplication If the same species S is involved in several different biological processes, S may either be represented by a single visual representation and linked to all involved processes, or it may be represented by multiple visual representations, each linked only to some processes. In any case, each path through S defines a connectivity between the involved processes.

However, it may be the case that some processes involve the same species, but that species' role is completely unrelated between the two processes. This is the case, for instance, if the processes involve different physical instances of that species, if the species is available in such abundance that the actual physical instance is irrelevant, or if the species is merely an unimportant byproduct.

Thus, if a species S is involved in multiple processes, we need to assess between which of these processes there exists in fact a *true connectivity* via S; or which merely involve S in different, unrelated contexts (*false connectivity*). True connectivity should be represented in the network structure and the visual diagram as a path through S. There should be no edges implying false connectivity. False connectivity can be resolved by introducing another visual representation for S and re-attaching any incident edges. We refer to this procedure as *node duplication*.

These considerations are important for finding a faithful diagram layout. If the number of involved processes is large, having only a single graphical representation may lead to a high amount of visual noise in the diagram: there may be a large number of edges, covering a long distance and linking actually completely unrelated processes. Having many independent representations certainly makes it easier to avoid visual noise. However, connections between different subgraphs may no longer be encoded explicitly, omitting crucial information from the diagram.

The criteria for deciding between true and false connectivity, and thus node duplication are not immediately clear. In practise, the decision is made by experts case-by-case, or general heuristics are employed (see Related Work). In this work, we aim for a more precise approach to decide node duplication automatically in the context of disease maps.

2.4 Biological Databases and Ontologies

Different research projects on the same organism or disease deal in principle with the same universal sets of biological entities and relationships. For instance, if two projects were to describe the metabolic network of *E. coli*, both are likely to mention the function of Adenosine Triphosphate (ATP), a basic molecule that appears in many metabolic reactions. Both projects use the same notion of ATP and its effects, yet they may describe it differently, e.g., by its full name, abbreviation or chemical formula. This hinders knowledge transfer and -integration. We are striving towards a structured, formalised body of knowledge for representing information about physical entities such as molecules, but also on biological terms describing processes (e.g. "glycolysis"), localisation (e.g. "cytoplasm") or functions.

There are several publicly available databases that gather information on biological entities such as proteins (*UniProt* [6]), genes (*EntrezGene* [5]) or drugs (*DrugBank* [11]). These databases often gather basic information and related research about the entity.

Likewise, biological terms describing processes, functions or cellular localisation can be represented in an *ontology*, a (directed acyclic) graph of terms and their relationships. For instance, the terms "glycolysis" and "carbohydrate metabolic process" may be connected by a *involved-in* relationship. The Gene Ontology project [12] provides three distinct ontology graphs describing molecular functions, cellular component or biological processes. Each ontology graph loosely describes a relationship, however, links between hierarchies may also exist, for instance that the DNA repair process occurs in the Mitochondrion.

2.5 Supervised Learning for Classification

Our goal is to predict whether a species alias in a disease map should be duplicated or not. For each species alias, we extract *features*, which we deem to be characteristic for the target label of the node (see Feature Engineering). Additionally, we are given training data in the form of one or several disease maps and a binary label for each species alias describing whether it was duplicated during manual curation. We aim to use this training data to fit a machine learning model such that it will be able to make meaningful predictions for species aliases in other disease maps.

We are working in the setting of *supervised learning*, which we briefly introduce in the following [13, 14]: We consider n observations $\mathcal{T} = \{(\mathbf{x}_i, y_i)\}_{i=1}^n$ (also called *training data* or *examples*) to be drawn from an (unknown) distribution P over $\mathcal{X} \times \mathcal{Y}$ where $\mathcal{Y}$ is the label domain and $\mathcal{X}$ is the feature domain. For the scope of this work, we restrict ourselves to the *binary classification problem*, i.e. $\mathcal{Y} = \{0, 1\}$. We assume that $\mathcal{X} = \mathbb{R}^d$ and the number of dimensions d is large. Let us denote the set of observed *ground-truth* labels as $\mathbf{Y} := \{y_i\}_{i=1}^n$ and the set of observed feature vectors as $\mathbf{X} := \{x_i\}_{i=1}^n$. $\mathbf{X}$ can also be seen as a matrix in $\mathbb{R}^{n \times d}$. We assume that labels are generated by an unknown function f such that $y_i = f(\mathbf{x}_i)$. Further, we are given a *loss function* $\mathcal{L} : \mathcal{Y} \times \mathcal{Y} \to \mathbb{R}$ that describes how different a prediction is from the true outcome. In general, we aim to find a (parameterised) function $\tilde{f}$ that minimises the *true risk* $\mathcal{R}(\tilde{f}) := \mathbb{E}_P \left[\mathcal{L}(y_i, \tilde{f}(\mathbf{x}_i))\right]$, where $\mathbb{E}_P$ is the expected value over P. Since the original distribution P is unknown, we instead seek to minimise the *empirical risk* on the training data $\mathcal{R}_{\text{emp}}(\tilde{f}) := 1/n \sum_{i=1}^n \mathcal{L}(y_i, \tilde{f}(\mathbf{x}_i))$ and assume the empirical risk approximates the true risk. In the following, we call a concrete choice of $\tilde{f}$ a *model* or a *classifier*. $\tilde{f}$ is commonly parameterised by a set of *model parameters* θ.

2.6 Graph Neural Networks

A possible family of models that can be employed for classification are *neural networks*. We introduce neural networks by example of one of its simples variants, the *multilayer perceptron*, or *fully-connected neural network* *. We then introduce the notion of convolutions on grid-structured data and proceed to generalise the intuition to graph-structured data, yielding the class of Graph Neural Network models. We proceed to describe how GNN models can be used for node classification.

Neural Networks The most basic building block of any neural network is a single *neuron*, which is given as the composition of a linear transformation with a nonlinear *activation function* σ. Formally, for a single input vector $\mathbf{x}_i$, the output of a single neuron is given by $\sigma(\mathbf{x}_i^T \mathbf{w} + \mathbf{b}_i)$ where $\mathbf{w}$ are called the *weights* of the linear transformation and $\mathbf{b}$ is the *bias*. The stacking of multiple neurons, of which each takes $\mathbf{x}_i$ as input, constitutes a *fully-conntected* or *dense layer* in a neural network. If inputs and weights are stacked in matrices $\mathbf{X}$ and $\mathbf{W}$, respectively, the output of a single layer is given by $\sigma(\mathbf{X}^T \mathbf{W} + \mathbf{b})$ where σ is applied element-wise. A neural network is obtained by stacking multiple layers sequentially such that the output of one layer is the input of the next layer. The output of an intermediate layer is often called *latent* or *hidden representation*. Formally, if $\mathbf{H}^{(i)}$ is the output of the i-th layer, then the output of the $i + 1$-th layer is given as

$$\mathbf{H}^{(i+1)} = \sigma((H^{(i)})^T \mathbf{W}^{(i+1)} + \mathbf{b}^{(i+1)}). \tag{2.1}$$

* A comprehensive introduction can be found in Zhang et al. [15]

Training The layer weights $\Theta = \{\mathbf{W}^{(1)}, ..., \mathbf{W}^{(l)}\}$ are considered to be the model parameters θ in the sense of the supervised learning framework described in Section 2.5. We aim to find a set of parameters such that the empirical risk is minimised. This objective can be optimised by *Gradient Descent*: We iteratively adjust the weights $\mathbf{W}^{(i)}$ such that the model prediction is improved with respect to the empirical risk $\mathcal{R}_{\text{emp}}$ [†]. More precisely, we consider the partial derivative of $\mathcal{R}_{\text{emp}}$ with respect to each weight matrix, which can be determined via the chain rule, and iteratively update the weights for a maximum number of steps or until the risk no longer improves. We can additionally specify the step size by a given *learning rate* η. Formally, in each step, also called *epoch*, we set

$$\mathbf{W}^{(i)\prime} \leftarrow \mathbf{W}^{(i)} - \eta \frac{\partial \mathcal{R}_{\text{emp}}}{\partial \mathbf{W}^{(i)}}.$$

Hyperparameters Characteristics such as the number of layers, the number of neurons in each layer, the choice of loss function and learning rate determine the *model architecture* and are sometimes called *hyperparameters*. The proper choice of hyperparameters is essential to the performance of the model and often determined empirically via search techniques.

Automatic Feature Extraction and Message-Passing In practise, selecting suitable features is in itself a substantial step in the process of finding a well-performing classifier. Particularly in high-dimensional domains, feature selection is not trivial. Consider the use-case of trying to find a model that, given a grayscale pixel image of dimensions (w, h), classifies the image based on whether it depicts a dog or a cat. It is not trivial how to manually extract features (criteria) from the image that are predictive of the target class. A straightforward approach would be to consider the brightness value of each input pixel as a feature, i.e. $\mathbf{x}_i \in \mathbb{R}^{w \cdot h}$. However, intuitively, looking at each pixel in isolation is unlikely to be useful since certainly the target class depends on the values of pixels *in their context*. Further, note that the hidden representation of some input (e.g. given by **??**) may be considered an alternate feature representation of this input. In this sense, neural networks can be thought to perform *automated feature extraction*.

Convolutions on Grids For sake of intuitive appeal, let us further entertain the example of classifying pixel graphics [‡]. It is important to note that we have additional information on the structure of the input, namely that its pixel values are arranged in a grid. This means there is a well-defined notion of context, or *neighbourhood*. Aggregating information across a local neighbourhood may enable a model to capture not only characteristics of individual pixels but higher-order patterns. To faithfully extract local patterns, the aggregation operation should be *local* (the aggregation considers only a part of the input image) and *translation invariant* (the aggregation should respond similarly to the same input patch, regardless to where it is positioned in the entire grid). In the context of neural networks, such an aggregation is called a *convolution* [15]. In the case of linear aggregation and grid-structured data, we can express a convolution operation on pixel $\mathbf{H}_{i,j}$ as

$$\mathbf{H}_{i,j} = u + \sum_{a=-\Delta}^{\Delta} \sum_{b=-\Delta}^{\Delta} \mathbf{V}_{a,b} \mathbf{X}_{i+a,j+b} \tag{2.2}$$

where u is the bias, and Δ is the (window) *size* of the *convolution kernel* $\mathbf{V}$. Note that the kernel can be any computation adhering to the constraints of locality and translation invariance. **??** describes a *convolutional layer* and a neural network containing such layers is called a *convolutional neural network* (CNN).

In image classification, a single input to the neural network is typically an entire image (a collection of pixels), and the convolution operator is applied to each pixel. Successive application of convolutional layers, potentially with different kernels can be thought to aggregate increasingly higher-order patterns in the input data. The extracted patterns can be considered intermediate, higher-order feature representations and the

[†] In the context of neural networks, $\mathcal{R}_{\text{emp}}$ is also sometimes called the total *loss*. This should not be confused with the loss function $\mathcal{L}$.

[‡] Analogous formulations can be used for other kinds of structured data, including 1-dimensional grids (sequences) such as RNA and DNA sequence alignments [16][17].

successive convolution operations extract increasingly higher-order features. Since a kernel computes a value for a given pixel based on the features of itself and its neighbours, we can interpret the operation of a kernel to perform *message-passing*: Neighbour nodes construct and transmit messages to the target node, which are then combined with the target node's features into the final output.

Convolutions on Graphs We extend the notion of a convolution quite from grid-structured graphs to arbitrary graphs. We will see that the convolutions considered here are trivially local and translation invariant. The key differences are that the order and the size of the neighbourhood is no longer fixed. As such, a potential aggregation must be *node-order equivariant*.

Let us consider an attributed graph G with node set V. Let $\mathbf{h}_i$ be the (intermediate) feature representation of vertex $v_i \in V$. Let $\mathcal{N}(v)$ be some neighbourhood of $v \in V$. Typically, $\mathcal{N}(v)$ is chosen as the 1-hop adjacency in G. However, note that different notions of neighbourhood can also be applied, so the input graph must not necessarily correspond directly to the computation graph that defines how messages are passed [§]. We can describe a simple convolution operation on attributed graphs as follows: the new latent representation $\mathbf{h}'_i$ of v_i is based on messages received by its neighbours. Each neighbour encodes its features by means of a function Msg. These messages are aggregated using a permutation-invariant aggregation function Agg. Finally, the neighbours' input and the node's own features $\mathbf{h}_i$ are coalesced via an update function Update into the new latent representation $\mathbf{h}'_i$. To summarise:

$$\mathbf{h}'_i \leftarrow \textsc{Update}(\mathbf{msg}_{ii}, \textsc{Agg}(\{\textsc{Msg}(\mathbf{h}_j, \mathbf{h}_i) \mid j \in \mathcal{N}_i\})) \tag{2.3}$$

Concrete choices of Msg, Agg and Update give implementations of *graph convolution layers*. A neural network containg such layers is commonly called a *graph neural network* (GNN) or *graph convolutional network* (GCN).

In simple GNN architectures, Msg is a linear feature extraction and depends only on the sending node, i.e. $\textsc{Msg}(\mathbf{h}_j, \mathbf{h}_i) = \mathbf{W}\mathbf{h}_j =: \mathbf{msg}_j$ for some learnable weight matrix $\mathbf{W}$. Note that like the kernel parameters $\mathbf{V}$ in **??**, these weights are shared among message-passing steps.

Update is the application of a non-linear activation function and Agg is given by

$$\textsc{Agg}(\ldots) = \bigoplus_{j \in \mathcal{N}_i} \alpha_{ij} \mathbf{msg}_j,$$

where α_{ij} is a coefficient determing the importance of $\mathbf{msg}_j$.

The framework of **??** produces a hidden feature representation for each node. This is the basis for solving node-level tasks such as the classification of clustering of individual nodes. Another common use case is to make a prediction for the entire input graph, the most prominent example in context of life sciences being molecule graphs. In this case, we want to aggregate all node features to produce a single value describing the input graph. Such an aggregation is called a *pooling* layer. This can be done either by application of a simple permuation-invariant aggregation function such as minimum, maximum, etc. or by iteratively coarsening the graph together with its node-level feature representations [19].

Simple GNN The *GCN layer* [¶] as proposed by Kipf and Welling [20] defines α_{ij} as a constant depending on the degrees of v_i and v_j, namely $\alpha_{ij} := 1/\sqrt{d_i d_j}$.

GNNs with Attention The *Graph Attentional Layer* (GAT) [21] allows the importance score to be learnable, i.e. adjusted via backpropagation and gradient descent during network training. An attention mechanism A determines the importance e_{ji} of $\mathbf{msg}_{ji}$. If the neighbourhood $\mathcal{N}_i$ is defined as the 1-hop-neighbourhood in the input graph, this can also be interpreted as the importance of edge (v_i, v_j). In its prototypical formulation,

[§] For instance, GraphSAGE [18] samples a fixed number of adjacent nodes.
[¶] The naming here is unfortunately ambiguous.

A is a single-layer fully-connected neural network with learnable weights $\mathbf{a}$ and activation function σ_{att}, as described in **??**. A receives both the feature representations of v_i and v_j as input, combined by concatenation:

$$e_{ij} := A(\mathbf{msg}_i, \mathbf{msg}_j) = \sigma_{\text{att}}(\mathbf{a}^T(\mathbf{msg}_i \| \mathbf{msg}_j)) \tag{2.4}$$

Importance scores e_{ij} are then normalised via the *softmax* function:

$$\alpha_{ij} := \text{softmax}_{j \in \mathcal{N}_i}(e_{ij}) := \frac{\exp(e_{ij})}{\sum_{k \in \mathcal{N}_i} \exp(e_{ik})}. \tag{2.5}$$

Attention is a technique that has previously been used successfully in other neural network architectures. In particular, Graph Attention Networks are analogous to the Transformer architecture [22] that has achieved great popularity particularly in areas of Natural Language Processing such as machine translation. For translation from a source language to a target language, text input is typically given as two sequences of tokens. The key idea behind the Transformer architecture in NLP is to apply an attention mechanism to assess the importance of other words in the source or target sequence with respect to the current word. Note that while the Transformer architecture relies heavily on the attention mechanism, it also directly implements the idea of message-passing based on known relationships between atomic inputs.

(diag-surfaces) on paper

Figure 2.3: Including known structure into the ML model as predictive bias.

Neural Networks as Classifiers Intermediate layers of neural networks can be interpreted to compute useful feature representations. One way to obtain a classification prediction from a neural network is to use these intermediate representations as an input to another off-the-shelf classifier (such as Support Vector Machines, for instance [23]). Another, more common approach, however, is to design the network such that the last layer contains one ouput neuron for each target class. Given some input $\mathbf{x}$, the output value of the i-th neuron expresses the estimated probability that $\mathbf{x}$ is of class c_i. To produce values in $[0, 1]$, the results of the final layer are normalised, e.g. with the *softmax* function (see **??**).

In order to train the neural network for classification, we need a loss function $\mathcal{L}$ to assess the quality of the prediction. We introduce the *Binary Cross Entropy* loss from the viewpoint of maximum likelihood estimation (based on [15]) but note that it can also be derived via the notion of cross-entropy. Generally speaking, we seek to estimate parameters Θ of an assumed probability distribution P given some observed data X. The method of *maximum-likelihood estimation* postulates that we should pick the parameters such that the observed data is most likely (i.e. occurs with highest probability) under P. The likelihood w.r.t.parameters Θ is measured by a *likelihood function* $L(\Theta)$. Formally, we aim for

$$\hat{\mathbf{\Theta}} = \text{argmax}_{\Theta} P(X \mid \Theta) = \text{argmax}_{\Theta} L(\Theta) \tag{2.6}$$

Because of connections to entropy and computational convenience, we instead consider the negative logarithm:

$$\hat{\mathbf{\Theta}} = \text{argmin}_{\Theta} - \log L(\Theta) \tag{2.7}$$

Looking at the negative log-likelihood in more detail directly yields the *Binary Cross-Entropy loss*. For notational convenience, let $\mathcal{Y} = \{0, 1\}$. Let $\pi_i = P_\Theta(y_i = 1 \mid \mathbf{x}_i)$ be the estimated probability that $\mathbf{x}_i$ belongs to class y_i. Since we are dealing with binary classification, we have $P_\Theta(y_i = 0 \mid \mathbf{x}_i) = 1 - P_\Theta(y_i = 1 \mid \mathbf{x}_i)$. Under

the assumption that input samples are independent and identically distributed, we have

$$\begin{aligned} -\log L(\Theta) &= -\log \prod_{i=1}^{n} (\pi_i)^{y_i} \cdot (1-\pi_i)^{1-y_i} \\ &= -\sum_{i=1}^{n} y_i \log(\pi_i) + (1-y_i)\log(1-\pi_i) \\ &= \sum_{(\mathbf{x},y)\in\mathcal{T}} \mathrm{CE}(f(\mathbf{x}), y) \end{aligned}$$

where CE is the cross entropy loss and $\mathcal{T}$ is the set of training data. In summary, minimising the cross entropy loss is equivalent to maximising the likelihood.

2.7 Support Vector Machines

Support Vector Machines (SVMs) are a family of supervised machine learning models typically used for binary classification. In this section, we present the basic derivation of SVMs with the motivation of providing intuition behind the *cost* hyperparameter and choice of kernel functions and their parameters. We refer to Tibshirani, Friedman, and Hastie [24] for a more rigorous and thorough treatment.

Support Vector Machines are linear classifiers: The basic idea is to find a hyperplane in the (possibly transformed) feature space $\mathcal{X}$ that best separates the training data w.r.t.its ground-truth class assignments.

Preliminaries For sake of notational convenience, let $\mathcal{Y} = \{-1, 1\}$. A *hyperplane* is an affine set of points $L := \{\mathbf{x} \mid \mathbf{x}^T\beta + \beta_0 = 0\}$. The signed distance from a point $\mathbf{x}$ to L is given by $d(x, L) := 1/\|\beta\|(\mathbf{x}^T\beta + \beta_0)$. Based on L, we can define a linear classifier

$$h_L(\mathbf{x}) = \mathrm{sign}(\mathbf{x}^T\beta + \beta_0). \tag{2.8}$$

$\mathbf{X}$ is *linearly separable* if there exists a hyperplane L such that $h_L(\mathbf{x}_i) = y_i$ for all $\mathbf{x}_i \in \mathbf{X}$. L is then called a *separating* hyperplane, or *decision boundary*.

Linearly separable case For now, assume that $\mathbf{X}$ is linearly separable. We wish to find a suitable separating hyperplane. One possible approach would be to minimise the distance of misclassified points to the hyperplane. Doing so by gradient descent yields the *perceptron training algorithm*. However, we are not guaranteed a unique solution. Further, if $\mathbf{X}$ is not linearly separable, the algorithm will not converge at all. Another possible approach is to search for a hyperplane that maximises the *margin* $\gamma(L)$ w.r.t.$\mathbf{X}$, i.e. the distance from the hyperplane to the closest point:

$$\gamma(L) := \min_{x\in\mathbf{X}} 1/\|\beta\| \left|\mathbf{x}^T\beta + \beta_0\right|. \tag{2.9}$$

The maximum-margin separating hyperplane is unique. Further, it seems reasonable to assume that a maximum-margin separating hyperplane will do well in generalising to unseen points. We aim to find a hyperplane $L(\beta, \beta_0)$ that achieves:

$$\begin{aligned} \underset{\beta,\beta_0}{\text{maximize}} \quad & \gamma(\beta, \beta_0) \\ \text{subject to} \quad & y_i(\mathbf{x}_i^T\beta + \beta_0) \geq 0; i = 1, \ldots, n \end{aligned} \tag{2.10}$$

Since L and γ are scale invariant, i.e. $\gamma(\beta, \beta_0) = \gamma(\lambda\beta, \lambda\beta_0)$ for any $\lambda \neq 0$, we can assume $\gamma(\beta, \beta_0) = 1/\|\beta\|$, i.e. $\min_{x\in X}\left|\mathbf{x}^T\beta + \beta_0\right| = 1$. **??** is then equivalent to

$$\begin{aligned} \underset{\beta, \beta_0}{\text{maximize}} \quad & 1/\|\beta\| \\ \text{subject to} \quad & y_i(\mathbf{x}_i^T \beta + \beta_0) \geq 0; i = 1, \ldots, n, \\ & \min_{x \in X} \left| \mathbf{x}^T \beta + \beta_0 \right| = 1 \end{aligned} \tag{2.11}$$

and can simplified further to

$$\begin{aligned} \underset{\beta, \beta_0}{\text{minimize}} \quad & \|\beta\| \\ \text{subject to} \quad & y_i(\mathbf{x}_i^T \beta + \beta_0) \geq 1; i = 1, \ldots, n \end{aligned} \tag{2.12}$$

General case Let us now consider the case that $\mathbf{X}$ is not linearly separable. In this case, there is no solution to the optimisation problems given above. However, we can relax the constraints so that some data points are allowed to lie inside the margin. We achieve this by introducing *slack variables* $(\xi_1, ..., \xi_n)$ to the optimisation constraints that express the allowed violation:

$$\begin{aligned} \underset{\beta, \beta_0}{\text{minimize}} \quad & \|\beta\| \\ \text{subject to} \quad & y_i(\mathbf{x}_i^T \beta + \beta_0) \geq 1 - \xi_i, \\ & \xi_i > 0, \\ & \sum_{i=1}^{n} \xi_i \leq K \end{aligned} \tag{2.13}$$

where K is some constant.

This optimisation is effectively solved by first transforming it into an equivalent problem known as its *Langrangian Dual*. To this end, it is convenient to express **??** as

$$\begin{aligned} \underset{\beta, \beta_0}{\text{minimize}} \quad & 1/2\|\beta\|^2 + C \sum_{i=1}^{n} \xi_i \\ \text{subject to} \quad & y_i(\mathbf{x}_i^T \beta + \beta_0) \geq 1 - \xi_i, \\ & \xi_i > 0 \end{aligned} \tag{2.14}$$

The *cost* hyperparmeter C can be interpreted as a tradeoff coefficient between the cost of margin violations and simplicity of the decision boundary. For large C, margin violations will be punished more strictly. For small C, violations may be allowed to achieve a hyperplane with lower norm, i.e. smoother decision boundary.

The Kernel Trick For most non-trivial classification problems, the classification function f we seek to approximate is not linear. A method to move beyond linearity but nevertheless use linear classifiers is to transform the input features $\mathbf{X}$ into a higher-dimensional space $\mathcal{X}'$ via some transformation Φ. Depending on the choice of Φ, $\mathcal{X}'$ may be of very high or even infinite dimensionality. Thus, computing Φ explicitly is sometimes not an option. Luckily, we will see that in case of Support Vector Machines, all we need is an inner product $\langle \cdot, \cdot \rangle$ in $\mathcal{X}'$. In the following, instead of some feature vector $\mathbf{x} \in \mathcal{X}$, we consider a transformed feature vector $\Phi(\mathbf{x}) \in \mathcal{X}'$. Let's inspect the most central equations for computing SVMs. First, consider the

Lagrangian Dual of **??** given by

$$L_D = \sum_{i=1}^{n} \alpha_i - \frac{1}{2} \sum_{i=1}^{n} \sum_{j=1}^{n} \alpha_i \alpha_j y_i y_j \langle \Phi(\mathbf{x}_i), \Phi(\mathbf{x}_j) \rangle$$

$$\text{where} \quad \alpha_i = C - \mu_i$$
$$\forall i: \quad \alpha_i, \mu_i \geq 0$$

Further, the decision function h_L (see **??**) can be rewritten as

$$\begin{aligned} h_L(\Phi(\mathbf{x})) &= \Phi(\mathbf{x})^T \beta + \beta_0 \\ &= \Phi(\mathbf{x})^T \left[\sum_{i=1}^{n} \alpha_i y_i \Phi(\mathbf{x}_i) \right] + \beta_0 \\ &= \sum_{i=1}^{n} \alpha_i y_i \langle \Phi(\mathbf{x}), \Phi(\mathbf{x}_i) \rangle \quad + \beta_0 \end{aligned}$$

The key point here to note is that Φ appears only in the context of inner products. This means we can avoid even specifying Φ explicitly and instead use a *kernel function* K that expresses the inner products in the transformed feature space:

$$K(\mathbf{x}, \mathbf{x}') = \langle \Phi(\mathbf{x}), \Phi(\mathbf{x}') \rangle.$$

K is a valid kernel function if its Gram matrix is positive semidefinite.

One popular choice is the *radial basis function* (RBF) kernel[‖], also called *Gaussian* kernel. Recall that a kernel function can be interpreted as a measure of similarity between its two arguments $\mathbf{x}$ and $\mathbf{x}'$. The RBF kernel implements this notion as a decaying function of their distance. If $\mathbf{x}$ and $\mathbf{x}'$ are similar, their distance will be small and $-\gamma \|\mathbf{x} - \mathbf{x}'\|^2$ will be relatively large. The decaying characteristic is implemented by the application of the exponential function. Thus, we can define the RBF kernel as

$$K_{\text{RBF}}(\mathbf{x}, \mathbf{x}') = \exp(-\gamma \left\| \mathbf{x} - \mathbf{x}' \right\|^2). \tag{2.15}$$

Since the distance is symmetric, K_{RBF} can be interpreted as a bell-shaped function. The hyperparameter γ controls the width of the bell shape, with larger values producing a more narrow shape.

2.8 Evaluation of classifiers

SVMs as well as GNNs are trained to optimise some specific function w.r.t.the training data. However, when comparing and selecting models, we need an unbiased performance measure that is based only on data and ground-truth labels.

The classifiers considered here will output a probability (or *confidence score*) that a given data point will belong to the positive class. To obtain a concrete, binary classification, we have to draw a *decision threshold* τ. If the predicted confidence score of a given data point is greater than τ, it will be assigned the positive class, else the negative class. In Table 2.1 we introduce some basic terminology for subsets of training data based on their true and predicted class.

Based on the terms in Table 2.1, we can define the following measures:

[‖] This is in fact an example where the transformed feature space is of infinite dimension: It can be seen via Taylor expansion that K_{RBF} is based on an infinite sum of polynomial kernels.

Table 2.1: Given a concrete, binary classification, the following terms describe (sizes of) subsets of the predicted data, depending on its ground-truth and predicted class.

	Predicted Positive (PP)	Predicted Negative (PN)
Actually Positive (P)	*True Positives* (TP)	*False Negatives* (FN)
Actually Negative (N)	*False Positives* (FP)	*True Negatives* (TN)

- *Accuracy*, given by the ratio of correctly classified examples: $\mathtt{TP+TN}/\mathtt{P+N}$. Note that for class-imbalanced data, this is not a sufficient measure, because misclassifications of the minority class will be underrepresented in the overall score.
- *True Positive Rate* (TPR), or *Recall*, given by $\mathtt{TP}/\mathtt{P}$ is the probability that a positive example will be predicted as such by the classifier.
- *False Positive Rate* (FPR), given by $\mathtt{FP}/\mathtt{N}$ is the probability that a negative example will be predicted falsely as positive.
- *Precision*, given by $\mathtt{TP}/\mathtt{PP} = 1 - \mathtt{FPR}$

A perfect classifier would yield a high True Positive Rate and a low False Positive Rate. Note that it is possible to trade-off FPR and TPR by varying the decision threshold. If the threshold is very high, only examples for which the classifier has high confidence will be actually assigned positive class. This means that the FPR will be low. However, then not all true positives may be picked up as such by the classifier, resulting in a low TPR . Lowering the decision threshold will increase TPR , but also potentially result in additionally picking up false positives, increasing the FPR .

The choice of the proper decision threshold, depends on the use-case since different importance may be assigned to either Precision or Recall. The original use-case of Nielsen et al.was to use a classifier trained for predicting node duplication to provide a low number of high-confidence examples as suggestions to the user. When considering only the few examples with the highest score, Precision is more important than Recall.

To assess the trade-off between FPR and TPR w.r.t.possible choices of classification threshold τ, we can plot FPR and TPR as a function of τ, yielding the *Receiver Operating Characteristic* (ROC curve).

As a heuristic for choosing τ, we can look for the threshold with the greatest distance between TPR and FPR at τ, i.e. $\tau_{\text{opt}} := \text{argmax}_{\tau \in (0,1)} \mathtt{TPR}(\tau) - \mathtt{FPR}(\tau)$.

Generally, a classifier could be considered better if its ROC curve leans towards the upper left, i.e. the area under the curve is greater. As such, we can compute the *Area Under Curve* (AUC) score given as

$$\text{AUC}(\tau) = 1/2(\mathtt{TPR}(\tau) - \mathtt{FPR}(\tau) + 1)$$

and define the optimal overall AUC score as $\text{AUC} := \text{AUC}(\tau_{\text{opt}})$. However, we acknowledge that reducing the performance of a classifier to a single number will hardly ever capture all characteristics and evaluation still depends heavily on the use-case.

3 Related Work

Of particular prominence is the work of Nielsen et al. [25].

3.1 Drawing Biological Networks

Tools Several tools exist for the curation and exploration of biological process diagrams, including *CellDesigner* [26], *Minerva* [27], and *Cytoscape* [28] and *VANTED* [29]. We refer to TODO for a comprehensive comparison.

3.2 Node Duplication

Related Notions Several other terms appear in the literature that are relevant for the problem at hand. A *currency metabolite* [30] is a metabolite that plays only a secondary role in most of the reactions it is involved in. This role may be to merely supply energy (i.e. act as "currency" in the metabolism) or act as some other form of catalyst. Commonly, currency metabolites appear in abundance in an organism, and often it is assumed that two reactions involving the same currency metabolite are not in fact linked stoichiometrically, i.e. linking these reactions via a common node would imply false connectivity. Prominent examples are molecules such as ATP or H2O. Currency metabolites are commonly duplicated. The notion of true connectivity is also reflected in the concept of *key connectors* [31]: because pathways in a metabolic network seldomly work in isolation, there necessarily will be connections between different pathways. Determining whether a bridging node between two pathways is indeed a key connector or merely describes false connectivity and should be split is the tricky part.

General methods While node duplication (also referred to as *Vertex Splitting*) has been treated from a theoretical perspective [32] [33], to the best of our knowledge there are relatively few concrete, general-purpose algorithm that employ automatic node duplication.

Most notably, Eades and de Mendonça N introduce a general graph drawing algorithm that applies node duplication to simplify the graph structure in order to find a better layout [34]. The method is an extension of the force-directed Kamada-Kawai algorithm [35]. Given a vertex v and an incident edge, they define a *tension* vector whose direction is the direction of the edge in the current drawing and whose magnitude is based on the difference between the actual edge length in the current drawing and some target distance. Any possible binary duplication defines a *split line* that partitions $\mathcal{N}(v)$ into two disjoint subsets $\mathcal{N}(v)^+$ and $\mathcal{N}(v)^-$. The *tension of a split line* is the sum of tensions of either $\mathcal{N}(v)^+$ or $\mathcal{N}(v)^-$ (they are in fact equal if the drawing is in equilibrium). The *tension of a vertex* then is the maximum tension of all possible split lines. In each iteration of the Kamada-Kawai algorithm, additionally, a vertex with tension greater than a given threshold is split into two duplicates according to its maximum tension split line. The choice of the threshold is left to the user.

Node Duplication has also been applied in the area of Electronic Circuit Design, for example to avoid edge crossings [36] or paths exceeding a maximum length [37] [38].

Henr, Bezerianos, and Fekete consider how to represent duplicates in a social network visualisation in which communities are represented by adjacency heatmaps [39].

Metabolic Models Because different instances of the same metabolite can participate in many different reactions, node duplication can be essential for working with metabolic models. While visualisation one possible motivation, node duplication also has to be considered for other tasks such as flux balance analysis or integration of secondary *-omics* data [40].

Node duplication in layout tasks potentially is a different problem from the general preprocessing since finding a good layout may come with particular constraints (such as considering edge crossings, stress etc.). However, the methods mentioned below do not take layout information into account when deciding node duplication and we thus make no explicit distinction here.

Since nodes and particular motifs carry semantic biological meaning, deciding node duplication in metabolic models poses additional challenges.

Any node v with degree greater than two introduces a connectivity between any two subsets of $\mathcal{N}(v)$. It is not trivial to distuingish whether a connectivity is *false*, i.e. only exists because participants in two reactions happen to be mapped to the same concrete node or *true* in the sense that the connectivity represents actually meaningful biological information.

Review A common characterisation is that a node shall be duplicated if its neighbourhood is highly heterogenous w.r.t some measure. In other words, a node should be split if it is involved in many different, unrelated processes as then it is assumed that in reality there are independent instances of that species, involved in the different processes independently.

One possible approach is to consider a graph-based centrality measure. If the target node has a very high centrality score, we make the assumption that then the node must necessarily be involved in different, unrelated processes, i.e. its neighbourhood is heterogeneous. For a concrete choice of centrality measure, early methods simply considered the node degree [41] [42]. Further work uses the Eigenvector centrality [40].

Other approaches make the notion of neighbourhood heterogeneity more explicit by characterising communities in the given network. A node then has heterogeneous neighbourhood, if it is incident to many different communities. Communities can be determined solely on the graph structure, for instance as induced by modularity maximisation [43]. Huss and Holme decide node duplication based on the contribution to overall modularity if the target node is removed [30]. Guimerà and Nunes Amaral classify nodes as different kinds of hub- or connector nodes based on their intra- and inter-community degrees, where communities are determined via modularity maximisaiton [44]. Communities can also be characterised by domain-specific biological knowledge, i.e. annotations that describe the cellular compartment [40] or the pathway [45] [46] for a given node.

Apart from the work of Nielsen et al., we are not aware of any other previous work that investigates using a classifier for node duplication.

Tools and Formats There are several tools that provide functionality to easily introduce duplicates once the decision has been made. *Arcadia* [47] allows to split a node such that each copy has exactly unit degree. *Omix* [48] makes it easier to introduce duplicates with certain connectivity patterns by providing a *motif stamp* tool.

One of the most common formats used for describing disease maps is an extension to SBML Level 2 given by *CellDesigner*. Further, SBML Level 3 now allows to attach layout information. Another prominent format is SBGN-ML.

3.3 Disease Maps

To date, disease maps have been created for a number of diseases, including Alzheimer's Disease (AlzPathway[49]), Parkinson's Disease (PDMap[7]), and recently COVID-19 [50]. Beyond serving as a platform for integrating existing knowledge, computational methods have been applied to, e.g., identify molecules and relations essential for the pathogenesis of Alzheimer's Disease [51].

[52]

Detailed information on the disease maps considered in this work can be found in Section 4.1.

3.4 Machine Learning on Biological Networks

The life sciences offer countless applications for machine learning methods. Herein, we constrain ourselves to methods that directly or indirectly work with network-structured data and apply neural network techniques, or are particularly relevant for this work. Further, for sake of brevity, we omit edge-level tasks such as link prediction in biological networks.

Applications of Graph Neural Networks

Applications of GNNs on biological are diverse in the formulation of the task, the underlying data (network and attributes) and the applied methods.

To the best of our knowledge, there is very little previous work that connects GNNs to graph drawing or even node duplication.

Tiezzi, Ciravegna, and Gori provide a method for layouting graphs using GNNs [53] . As a first approach, they train a GNN to draw graphs based on ground-truth examples obtained from other graph drawing software. As attributes, each node is assigned a positional encoding based on the Laplacian Eigenvectors of the graph. The loss function aims to minimise the distances from the produced drawing to the ground-truth drawing (modulo affine transformations). Further, inspired by optimisation-based methods such as Stress Majorisation [54], they employ a GNN to directly minimise the stress function on the predicted node coordinates. Note that the all-pairs-shortest-paths computation has to be done only during training. At inference time, the model predicts node positions based on the supplied positional encoding, which is potentially easier to compute. Additional quality measures, such as the number of edge crossings, can be included in the loss function without sacrificing the advantage that predictions only ever require the graph structure and positional encodings and no additional computation.

Node-level tasks You et al. [55] consider the problem of predicting the function of a protein based on its sequence. A current challenge is bioinformatics is the gap between the number of known protein sequences and the number of protein sequences annotated with a biological function (*sequence-annotation-gap*). You et al. suggest to consider each protein with respect to other proteins it is known to interact with. As such, they propose a GNN approach in which proteins are represented as nodes and connected based on information from Protein-Protein interaction databases. The function annotations here are in fact Gene Ontology terms (see TODO). Once the biological function is known, another challenge is to assess the functional similarity of two proteins. One way to approach this is to compare the (sets of) Gene Ontology terms of two given proteins. Zhong, Kaalia, and Rajapakse compute an embedding for GO terms based on the graph structure of the GO ontology [56]. These embeddings can be thought of to encode the term's position in the graph, that is, its relationship to other terms. A measure of semantic similarity can be derived by comparing the (sets of) computed embeddings.

Single-cell RNA-sequencing (scRNA-seq) is a technology that provides gene expression data on the level of individual cells. In the work of Ravindra et al. [57], each cell is represented as a node and features are its

gene expression data. Graph connectivity is defined on a node's k nearest neighbours. The goal is to predict whether a cell corresponds to a healthy or pathological disease state w.r.t to Multiple Sclerosis (MS). The motivation is to work towards developing a diagnostic test for MS based on scRNA-seq technology.

Graph-level tasks Graph Neural Networks have found highly successful applications for the problem of molecular property prediction. This is a graph-level task where the input is a *molecule graph* and we strive to predict specific chemical properties of this molecule. In a molecule graph, nodes represent atoms and edges represent bonds. Nodes and edges have attributes describing e.g. an atoms element, or the type of a bond. Properties to predict may include toxicity or antibacterial activity. This task is relevant particularly in the field of drug development where a large number of molecules has to be tested for potential usefulness as a drug (*virtual screening*). Traditionally, molecules were represented by *fingerprint vectors* which describe characteristics of the entire molecule such as the presence of functional groups. While these fingerprints may well serve as input to a neural network predictor, the structure of these fingerprints is designed manually and often not directly dependent on the prediction task. Graph Neural Networks provide the means to compute such fingerprints directly based on the the structure of the molecule and concrete, low level properties. Moreover, the extraction and aggregation of input features performed by graph neural networks is differentiable and thus the entire prediction pipeline can jointly be optimised end-to-end, yielding task-specific fingerprints. Stokes et al. use this approach to predict the growth inhibition against *E.coli*, eventually resulting in the discovery of experimentally verified potent antibiotics that are structurally different from known antibiotics [58]. Notably, Duvenaud et al. employ this approach well before the recent popularisation of Graph Neural Networks in the style of **??**. Focussed reviews of applications of GNNs for molecular property prediction [60] and drug development in general [61] can be found in the literature. Further, Baranwal et al. train a GNN model to compute fingerprints of molecules that are then used to predict their broad metabolic pathway class (e.g. carbohydrate metabolism, amino acid metabolism, *etc.*) [62].

Edge-level tasks GNNs have been applied for edge-level tasks particularly for the problem of link prediction in biological interaction networks. GNNs have been applied to predict interactions between diseases and drugs [63], interactions between drugs, proteins and drug side effects [64] and interactions between proteins [65]. Many other applications can be found in the literature [66].

Other relevant ML approaches

3.5 Semantic Representations

Gene Ontology

[67] [68]

Work exists to develop similarity measures between two GO terms, or two sets of GO terms (see Section 3). These are, by definition, pairwise similarity measures. These could be interpreted as distance measures and these distances could be considered directly in a machine learning model.

An alternative approach is to find a embeddings (vectors describing feature representations) of the given GO term s.t. the similarity of their embeddings is meaningful, i.e. reflects the similarities in the GO graph. In fact, some approaches for semantic similarity measures depend exactly on such embeddings.

Embeddings

4 Methods

4.1 Datasets & Preprocessing

Graph construction

Disease maps can be interpreted as bipartite graphs in a natural manner with the bipartite node sets being the set of interactions and the set of species, respectively. The disease maps considered in this work are given in an extension to SBML defined by the *CellDesigner* tool. The format is very rich in information and leaves some room for ambiguity concerning graph construction. In the following, we describe what we take into account to construct a graph.

The most central elements in an SBML model are the lists of reactions and species aliases (visual representations of species). An entry in the list of reactions carries references to species taking part in that reaction. Since different occurences of a species can be visualised as duplicate species aliases, each entry for a participating species additionally contains a reference to a specific species alias. Participating species are distuingished by the role they play in that reaction. Herein, we consider the basic roles defined by standard SBML: products, modifiers and reactants *. We create directed edges for reactants and products in the direction of the reaction. A modifier is attached by two edges, one in either direction. For computing structural node features and for message-passing, we sometimes also consider the bipartite projection. Herein, we compute the bipartite projection based on the undirected interpretation of the graph.

(graph-interpretation) from paper notes

(a) Illustration of how a rich SBML model is interpreted as a simple, directed graph.

todo: something illustrating CD-SBML structure / distinction between species and species aliases – or not at all? not really super relevant...

A species alias can either be simple or *complex* in the sense that it represents a container for other species aliases. This is used to represent e.g. biological complexes of proteins. Simple and complex species aliases are arranged in an arbitrarily nested hierarchy. For the graph structure, we consider only top-level elements, that is, we consider complex species aliases as single nodes and omit their contents †. A reaction may involve an entire complex species alias (CSA) or only a species alias contained in the CSA. Since we interpret the CSA as a single node, an edge will be attached to it in either case.

Species aliases can also be contained in *compartments* representing biological cellular compartments or broader notions of spatial relationship. We do not consider compartments at all herein (see Section 7).

Determining ground-truth Labels

Although numerous disease maps are publicly available, to the best of our knowledge none are explicitly annotated with a per-alias label indicating node duplication. In case we are given a sequence of reorganisation steps $(G_1, ..., G_k)$, we infer node labels by comparing successive steps G_t and G_{t+1}. In case we are given only a single disease map G, we first construct a collapsed version G_0 by collapsing any species aliases corresponding to the same species into a representative node and moving any edges incident to aliases to the corresponding representative. We then proceed by comparing G_0 and G like reorganisation steps. In order to make our results comparable to the work of Nielsen et al. [25], we employ the same algorithm for inferring ground-truth labels. Because the algorithm has received little explicit treatment in the original publication, we motivate and describe it here in detail for clarity.

* *CellDesigner* provides an even more fine-grained distinction of species participating in a reaction. Species can be *main* reactants or products, *modifiers* or *additional* reactants or products. We omit this for simplicity. See [69], ch. 2.4.

† Contents of complex species aliases will be taken into account when considering GO annotations, see TODO

A simple approach that comes to mind is to consider nodes newly introduced in G_{t+1} and look for a subset $W \subset V(G_{t+1})$ whose neighbourhood completely covers the neighbourhood of some node in G_t, i.e. $\bigcup_{w \in W} \mathcal{N}_{t+1}(w) = \mathcal{N}_t(v)$ for some $v \in G_{t+1}$. However, this does not suffice. It is important to note that we can make no assumptions about what manipulations were made to create G_{t+1} from G_t. In particular, nodes may have been removed, added or duplicated and edges may have been added, removed or re-wired. To deal with this, instead of finding the duplicates of a given node in G_t, the algorithm seeks to identify a possible *duplication parent* of a given node in G_{t+1}. The basic idea is that the neighbourhood of duplicates will be at least partially included in the neighbourhood of the duplication parent.

Intuitively, the algorithm works by starting at a given node $v_i \in V(G_{t+1})$, identifying its neighbour nodes in G_{t+1} and considering their neighbours in G_t. If v_i is a duplicate, we expect its duplication parent to be among these nodes.

Algorithm 1: Procedure to identify duplication parents. Transcribed from Nielsen et al. [25].
Data: Directed graphs G_t and G_{t+1} (reorganisation step), node $v_i \in G_{t+1}$
Result: Duplication parent of v_i or None

1 $W_+ \leftarrow \mathcal{N}_t^-(\mathcal{N}_{t+1}^+(v_i))$
2 $P_+ \leftarrow \mathcal{N}_{t+1}^-(\mathcal{N}_{t+1}^+(v_i)) \setminus W_+$
3 $W_- \leftarrow \mathcal{N}_t^+(\mathcal{N}_{t+1}^-(v_i))$
4 $P_- \leftarrow \mathcal{N}_{t+1}^+(\mathcal{N}_{t+1}^-(v_i)) \setminus W_-$
5 **if** $W_+ = \emptyset \vee W_- = \emptyset$ **then**
6 $P \leftarrow P_+ \cup P_-$
7 **else**
8 $P \leftarrow P_+ \cap P_-$
9 **if** $\|P\| = 1$ **then**
10 Let w be the single element in P
11 **return** w
12 **else**
13 **return** None

The procedure is given in pseudocode in **??**. For directed graphs, let the *positive neighbourhood* of v in G_k $\mathcal{N}_k^+(v)$ be given as $\{w \mid (v, w) \in E(G_k)\}$ an the *negative neighbourhood* $\mathcal{N}_k^-(v)$ as $\{w \mid (w, v) \in E(G_k)\}$. The set operations identify nodes solely based on their alias ID. This means that $V(G_t)$ and $V(G_{t+1})$ may potentially have nonempty intersection (indeed, the algorithm relies on it).

Line 8 states that a valid duplication parent must be reachable from both positive and negative direction. This is only relevant if there is no positive (resp. negative) neighbourhood shared between the reorganisation steps (which is also the case if the target node is a sink, resp. source). Line 6 takes this into account. Then, a duplication parent may still be uniquely identified if there is a single shared neighbour in the opposite direction (see Figure **??**). Line 9 handles cases when multiple candidate duplication parents exist and we cannot infer a unique single one (see example Figure **??**). The algorithm is able to identify duplication parents even if edges have been removed (see example Figure **??**).

subfig

(a) Example in which there is no shared positive neighbourhood. However, a unique duplication parent can still be identified because node 2 has unit out-degree.

subfig

(b) Example where a unique duplication parent cannot be identified due to ambiguity.

subfig

(c) Parents can still be inferred if edges are removed. Without node 7, however, the case would be ambiguous

subfig

(d) Ambiguities are resolved by considering both positive and negative neighbourhoods.

Figure 4.2: Examples for Algorithm **??**

Feature Engineering

In general, there are three aspects of a disease maps based on which features can be defined. The first is the *structural* aspect in which we use graph-theoretical measures to characterise species aliases (graph nodes) based on their connectivity in the network. This was considered in detail in the feature engineering step in the work of Nielsen et al. and was used in numerous approaches for metabolic networks (see Section 3).

The second aspect is *semantic*: species are annotated with biological domain knowledge, commonly in the form of links to databases that provide additional information about that species (see **??**). In this work, we aim to explore how to exploit Gene Ontology term annotations.

The third aspect is that of *layout*: Prior to making a prediction on node duplication, the disease map may already have been laid out to some extent. If so, positions of species aliases certainly carry some meaning. Which exactly, however, is unclear since positions are most likely determined by a mixture of layout requirements, semantic arrangement and preference of the curator.

For the scope of this work, we avoid using layout-based predictors since we only have one practical instance in which we have layout information and ground-truth labels available, which is when making a prediction for a AlzPathway reorganisation step and comparing it to the actual next step in the reorganisation sequence. However, this is the only disease map for which reorganisation steps are available and it is of limited size. Thus we decide to omit this approach for now, while acknowledging that considering layout information may lead to interesting approaches (see **??**) [‡].

Structural Features The following structural features were defined and used by Nielsen et al. and we re-implement them for comparability. Let $\sigma_{st}(v)$ denote the number of shortest paths from s to t passing through v and σ_{st} is the number of shortest paths from s to t. Since in the following, we always consider the graph to be undirected, σ is symmetric w.r.t s, t.

- `degree`: The degree of a node, counting both incoming and outgoing edges.
- `clustering_coefficient`: The *clustering coefficient* [70] for a node v is given as

$$\frac{2\tau(v)}{\deg(v)(\deg(v)-1)}$$

  where $\tau(v)$ is the number of possible triangles through v in the graph.
- `betweenness_centrality`: The *betweenness centrality* of v reflects the number of shortest paths that pass through v:

$$\sum_{s \neq v} \sum_{t \neq v} \frac{\sigma_{st}(v)}{\sigma_{st}}$$

- `closeness_centrality`: As used here, the *closeness centrality* for v is given by

$$\frac{\|V\| - 1}{\sum_{s \neq v \in V} d(s, v)}$$

  where $d(s, v)$ is the shortest-path distance from s to v.
- `eigenvector_centrality`: The *eigenvector* centrality is a measure of transitive importance of a node. The basic idea is that a node is important if it is linked to other important nodes. The centrality values of each node are given by the components of the principal eigenvector of the graph's adjacency matrix.

Additionally, in order to capture the characteristics of a node's direct neighbourhood, the following secondary features are computed:

[‡] We do consider layout information as a criterion for attaching edges to duplicates, see Section 4.3.

- `neighbour_centrality_statistics`: For node v, this the stacked vector of statistics over several centrality measures of neighbours of v. The statistics are mean, minimum, maximum and standard deviation. The centralities are betweenness, closeness and eigenvector centrality and degree.
- `distance_set_sizes`: A vector of length k in which the k-th entry is the normalised number of nodes exactly k hops from v. Here, $k = 5$ is considered. The values are normalised by the number of nodes reachable in a grid graph via k hops.

Except for the clustering coefficient, additionally all characteristics are also computed on the bipartite projection and included as separate features. Except for `distance_set_sizes`, all features are min-max-normalised w.r.t all given training graphs.

Additionally, we consider the directed degrees (`in_degree`, `out_degree`). This is motivated by the notion that a species alias may have a different biological meaning w.r.t node duplication if either in- our out-degree is higher, both are balanced or the node is a source or a sink.

Because the input networks are of nontrivial size (see Section 5.1), computation time has to be taken into account. Particularly attributes relying on global information (such as e.g. closeness centrality) can provide a challenge for high-level graph libraries such as *networkx* and may not complete in a reasonable amount of time. More sophisticated implementations working with a lower-level language such as those provided by the *igraph* library used herein show a significant speedup. Nielsen et al. additionally consider the centralities of a given node in its ego graphs of sizes 3 and 5. Due to time constraints, we omit this feature. We note that we achieve comparable classification performance as reported the original work even without using that feature (see Experiments & Results).

Semantic Features A simple semantic feature that Nielsen et al. propose is the one-hot-encoding the species type. Possible species types are *protein*, *RNA*, *simple molecule*, *ion*, *gene*, *phenotype*, *drug*, *complex*, *degraded* and *unknown*.

In addition, we explore using Gene Ontology term annotations to infer meaningful features. We hypothesize that, in general, a node should be duplicated if its neighbourhood is highly heterogeneous, i.e. the species alias establishes false connectivity between actually unrelated processes. Previous approaches commonly focus on structural or layout-based features. However, these facets involve domain knowledge only implicitly, if even. As a characterisation of neighbourhood homogeneity, we seek to explicitly include domain knowledge about what biological processes a species is involved in. To this end, we consider the Gene Ontology terms linked to each species in the given disease map. In particular, we consider those terms of the "*biological process*" subtree of the GO graph (see Section **??**).

We extract GO annotations directly from the given *CellDesigner*-SBML files.

Given a set of GO term annotations for a species alias, we have to derive a fixed-length numeric vector from them that can be used as a feature vector. We achieve this by computing an *embedding* vector for each GO term that reflects its position in the GO ontology graph and thus its semantics. We acknowledge that there is previous work developing pairwise similarity measures between GO terms (see Related Work). However, the direct, embedding-based approach has the following advantages:

- We are alleviated of the choice of an additional similarity measure (effectively leaving that problem to the classifier). This also means that, particularly in case of a GNN classifier, the neural network may potentially be able to capture more flexible relationships than what we would encode with some similarity measure.
- This gives us a simple approach for including annotation information for complex species aliases by combining the embeddings of the contained nodes.
- Since in the end we aim to assess the heterogeneity of a node's neighbourhood, the consideration of embedding values could be incorporated in the message-passing step of a neural network (see Outlook & Future Work). Further, node-level information may be useful for the task of finding an attachment of edges after duplication.

For computing an embedding vector for a given GO term, we closely follow the approach of Zhong, Kaalia, and Rajapakse [56] and encode a term's position in the GO graph via the *node2vec* algorithm.

The above considerations lead to the following concrete feature definitions:

- `GO_embedding`: The basic idea of this approach is to only provide an encoding of the term's position in the GO graph as node feature. A GNN model could then potentially capture characteristics of a target node's neighbourhood via its aggregation function.
- `GO_stddev`: We additionally try capturing neighbourhood heterogeneity by interpreting the embeddings as points in an euclidean space and deriving a measure for the spread of these points around their centroid (mean). The idea is inspired by the measure of standard deviation, i.e. the average squared distance from the mean. This can conventienly be expressed as the sum of variances over each dimension. Let $(\mathbf{x}_1, ..., \mathbf{x}_n)$ be the embeddings of neighbour nodes, and let $\bar{\mathbf{x}}$ be the centroid (i.e. dimension-wise mean). Assume the points lie in a D-dimensional euclidean space. Let $(\mathbf{x}_i)_k$ denote the k-th entry of $\mathbf{x}_i$. We then consider $\sigma = \sqrt{\sigma^2}$ as a measure of spread, given by

$$\begin{aligned}\sigma^2 &= 1/n \sum_{i=1}^{n} \|\bar{\mathbf{x}} - \mathbf{x}_i\|_2^2 \\ &= \sum_{d=1}^{D} 1/n \sum_{i=1}^{n} (\bar{\mathbf{x}})_d - (\bar{\mathbf{x}_i})_d)^2 \\ &= \sum_{d=1}^{D} \mathrm{Var}(\left[(\mathbf{x}_1)_d, ..., (\mathbf{x}_n)_d\right])\end{aligned}$$

  where $\mathrm{Var}(\left[(\mathbf{x}_1)_d, ..., (\mathbf{x}_n)_d\right])$ is the variance along dimension d. Note that this approach encodes characteristics of the embeddings across a node's neighbourhood directly into a single feature vector and can thus be used with any classifier, such as SVMs.

There are two cases when we are required to aggregate a set of embeddings into a single value. On the one hand, a single protein can be annotated with several GO terms. On the other hand, a complex species alias potentially contains muliple annotated aliases. In both cases, we take the mean.

4.2 Training & Classification

The basic pipeline is illustrated in Figure 4.3. The general approach is to extract data from the *CellDesigner*-SBML files describing some disease maps, and construct for each an attributed, directed, bipartite graph G. Additionally, we infer ground-truth labels for nodes in G. We aim to classify nodes in G. For each node, we compute a feature representation. For the SVM model, the feature vector and ground-truth label is the only input. For GNN models, additionally the network structure is given.

Nodes corresponding to complex species aliases and nodes of degree less than two are excluded from prediction. This means they will not be considered as input examples when training or evaluating the classifier. Note that these nodes are still part of G and potentially influence the features of other nodes. Further, excluded nodes will still participate in the message-passing steps of GNN models.

The set of thus constructed input graphs is partitioned into training and testing graphs. For the concrete choice of training and testing partitions, we explore different settings, see Experiments & Results.

(diag-pipeline) on paper

Figure 4.3: Basic pipeline

The task at hand comes with a particular set of challenges:

- Different disease maps potentially have very different characteristics (see e.g. the difference between AlzPathwayReorg or PDMap and ReconMap in Figure **??**), which may make it difficult for the model to generalise to unseen disease maps. We evaluate generalisation ability throughout our experiments.
- Typically, only a few nodes are duplicated (see Figure **??**). Thus, the positive class is underrepresented in the dataset. We have to ensure that model performance does not suffer due to class imbalance. We address this issue by considering two approaches: First, we undersample the majority class. Second, we provide class-specific weights to the ML models such that an example of the minority class will be assigned more importance.
- The ground-truth labels may not be perfectly reliable. For one, the decision whether a node was duplicated or not during curation is subjective to the expertise and preference of the curator. The criteria that were relevant to the curator are most likely not perfectly reflected in the features we provide the model with. Thus, it may be the case that some training examples are contradictory in label w.r.t.their feature representation. Further, considering several reorganisation steps is likely to introduce contradictory examples if a node is duplicated in some step but not in an earlier one.
- The number of datapoints used for training and evaluation is relatively low compared to other common use-cases for Machine Learning. Care has to be taken to avoid overfitting, i.e. the model adjusting overly well to the training data at the cost of prediction performance on validation data not seen during training. Further, particularly when partitioning the available data into subsets for training and testing, we have to make sure we still have plenty of representative examples in each subset. We address this issue in part by avoiding to split a disease map internally into training and testing subsets. Further, we want to highlight that SVMs an GNNs have been applied successfully on datasets of comparable size. Note also that the GNN architectures we considere herein are of much smaller complexity (in terms of number of model paramaters) than famous neural network architectures used in Computer Vision or Natural Language Processing and may thus not require a particularly large amount of training data to fit all parameters.

Experiments and results are given on Section 5.

4.3 Attachment of edges

Assume we are given a binary classifier that decides whether a node should be duplicated. If a node v is eligible for duplication, we next need to determine how many duplicates to introduce and how to distribute edges to and from v across the duplicates. Formally, we aim to find a partition of the neighbourhood of v. Based on the intuition that a good duplication is one that reduces the heterogeneity of the neighbourhood, we can characterise the partitions as *clusters* in the sense that intra-cluster distances are smaller than inter-cluster distances.

The choice of distance metric is open. Of particular interest are metrics that reflect semantic similarity of attached GO terms [§]. However, because in the given datasets, most aliases are annotated with a relatively large number of GO terms and exploiting these annotations for classification was problematic (see Experiments & Results), we opt for a simpler approach first and leave this open to future work. Instead, we consider the layout positions of aliases and their euclidean distances. Note that this approach is only applicable if layout information is actually given, i.e. this approach can not be used if we construct a collapsed graph from a single given disease map (unless we would infer layout information for the newly constructed, collapsed graph).

Particularly when considering euclidean distances in the layout, a suitable clustering algorithm needs to handle outliers in a sensible manner. Additionally, we do not know the number of clusters in advance. This eliminates basic partition-based methods such as k-Means and extensions. Further, we seek to assign all points to a cluster, i.e. we do not want to exclude any points as noise. Also, since different node neighbourhoods have potentially different scales, we aim to avoid having to specify hyperparameters like distance thresholds as they are used in density-based clustering algorithms like DBSCAN or Optics. A family of clustering

[§] Indeed, Ostaszewski et al. applied GO semantic similarity to cluster nodes in a disease map.

algorithms that seems well suited is that of *agglomerative* clustering: Initially, each point is assigned its own cluster. Iteratively, the two clusters with the smallest inter-cluster-distance are merged until only a single cluster remains. This yiels a hierarchical clustering tree, also called *dendrogram*, as depicted in Figure 5.10.

There are several canonical choices of distance measures between two clusters C_1 and C_2. The most simple ones employed for agglomerative clustering are:

$$\begin{aligned} \textit{single linkage:}\ & d(C_1, C_2) = \min_{p \in C_1, q \in C_2} d(p, q) \\ \textit{complete linkage:}\ & d(C_1, C_2) = \max_{p \in C_1, q \in C_2} d(p, q) \\ \textit{centroid linkage:}\ & d(C_1, C_2) = d(\text{mean}(C_1), \text{mean}(C_2)) \end{aligned}$$

where C_1 and C_2 are considered to be sets of points. Complete linkage and centroid linkage seem inadequate since they would be strongly affected by large in-cluster variances and do not work well if clusters are not convex.

Setting a threshold value on the maximum dissimilarity inside a cluster, we obtain a concrete clustering. This can be thought of as "cutting off" the dendrogram at a specific height. Note that here we do not have to specify the number of clusters but instead a threshold dissimilarity. This threshold can be determined automatically via a heuristic: We look for the strongest increase in the distance to the next closest cluster before each merge step. Formally, let $d = (d_1, \ldots, d_k)$ be the monotonically increasing sequence of inter-cluster distances at which a merge occured. The first discrete derivative d' of this sequence gives the step sizes while the second derivative d'' describes the change rate in step sizes. The index of the maximum in d'' yields the number of clusters. Note that we require $k \geq 8$ points for determining at least two values in the second discrete derivative. In case of $k < 8$, we fall back to the first derivative (step size). Examples show that this is a good approximation for a low number of points. As special cases, since the decision to duplicate is assumed to be already given by the classifier, we exclude the possibility of returning only a single cluster. If $\left\|\mathcal{N}(v)\right\| = 2$, then we always trivially split.

Note that thus we characterise the procedure to identify the number of clusters independently of the concrete scale of the data. However, we can see that this procedure strugges if intra-cluster variances are diverse an the internal variance of a cluster is close to another inter-cluster distance (see Figure 5.10). We accept this disadvantage for now and hypothesize it has little practical impact in this use-case.

4.4 Implementation

5 Experiments & Results

5.1 Datasets used for training and evaluation

A visual overview of the disease maps considered in this work is provided in Figure **??**.

The *AlzPathway* map describes signaling pathways related to Alzheimer's Disease. Since its initial publication [71], it has received several updates and further analyses [72, 49, 51]. The map has received additional curation focussing on increasing readability by means of reorganising existing network elements [73]. This includes the duplication of some species aliases. During curation, snapshots of intermediate progress (*reorganisation steps*) were saved. Note that the reorganisation steps are not atomic: each step includes modifications to several nodes and edges. This sequence of reorganisation steps served as the basis for the work of Nielsen et al. to train an SVM classifier to predict node duplication [25]. In this work, we consider these reorganisaton steps for training data (AlzPathwayReorg). Note that from the sequence of reorganisation steps, we exclude the steps that do not correspond to any duplication events. Further, we consider the last of the reorganisation steps, i.e. the final result as a single, independent map (AlzPathwayReorgLast).

The *PDMap* [7] describes the major pathways involved in the pathogenesis of Parkinson's Disease. The map can be explored via a hosted *Minerva* instance, reachable at `https://pdmap.uni.lu/minerva`. For this work, we consider the version of this map as exported from *Minerva* at 2021-09-07.

ReconMap [74] is a visual representation of the genome-scale metabolic model *Recon 2* [75] that aims to comprehensively model the human metabolism. It can be viewed at `https://vmh.life/minerva`.

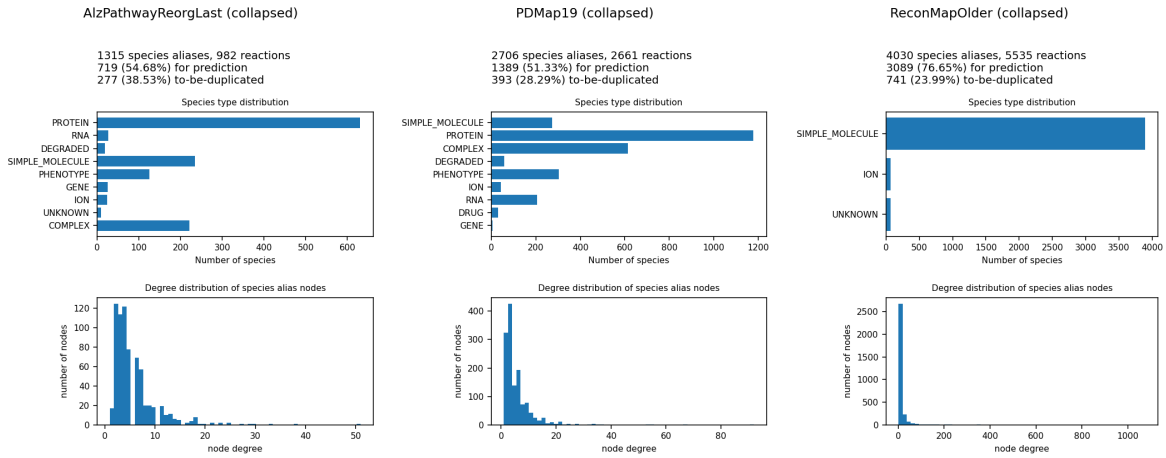

Figure 5.1: An overview of characteristics of the *collapsed* networks used for training. The count of species aliases and reactions is effectively the count of the bipartite node sets in the constructed graphs. Since we are consiering collapsed diagrams, the count of species aliases equals the count of species. Networks and labels are determined as described in Section 4.1.

5.2 Basic hyperparameter search

The models were trained on the AlzPathway reorganisation steps (AlzPathwayReorg) and evaluated on the Parkinson's Disease Map (PDMap).

Support Vector Machine

For the choice of kernel function, we pick the RBF kernel (see **??**) as a heuristic choice since Nielsen et al. showed that a generally best-performing kernel cannot easily be determined and showed that the RBF kernel generally achieves good performance. Since we use a different SVM implementation than Nielsen et al., that might potentially interpret the parameters slightly differently, for the choice of `C` and γ, we additionally perform grid search over the same ranges of values. The results are given in Table **??**.

Table 5.1: Considered SVM hyperparameters, value range searched via grid search and best identified combination of values.

Hyperparameter	*Searched range*	*Choice*
Cost (C)	2^{-9} to 2^{3}	0.5
Gamma (γ)	2^{-3} to 2^{9}	0.1

Graph Neural Network

The range of searched hyperparameters is based on the work of You, Ying, and Leskovec who systematically evaluated choices of hyperparameters for various tasks [76]. They suggest a constrained design space for Graph Neural Networks for tasks such as node classification.

Table 5.2: Considered hyperparameters for the GNN models. In case there are multiple possible values, the best hyperparameter combination is given in the third column.

Hyperparameter	*Searched range*	*Choice*
Dropout	`[0.0, 0.1,0.2,0.4]`	`0.0`
Aggregation function	`[add, mean, max]`	`add`
Fully-connected layers before message-passing	`[1,2]`	`2`
Fully-connected layers after message-passing	`[2,3]`	`2`
Message-passing layers	`[2,4,6,8]`	`2`
Connectivity	`[skip_sum, skip_cat]`	`skip_sum`
Activation function σ	`[PReLU]`	
Use batch normalisation?	`[yes]`	
Learning rate η	`[0.01]`	
Optimiser	`[adam]`	

5.3 Reproducing previous work & Comparison to GNN

In this section, we reproduce the original task from Nielsen et al.using an SVM classifier. Additionally, we introduce a simple GNN classifier that operates on the same input data as the SVM, using the bipartite projection of the disease map graph for message-passing (see Section 4.1). Further variants and extensions of the GNN model will be evaluated in the following sections.

The models were trained on the AlzPathway reorganisation steps (AlzPathwayReorg) and evaluated on the Parkinson's Disease Map (PDMap) and on *ReconMap*.

To avoid actually overfitting, for overall performance evaluation, we consider the model state at the training epoch that performs best on the validation split. This is not necessarily the best epoch w.r.t.the training split, see Figure **??**. The tradeoff can also be seen in shape of imperfect performance on the training split in the ROC curves. Note that, in practise, a ML model should be able to reliably generalise to data that was not observed during the process of finding and tuning a model. Usually, this is done by splitting the available data into three parts: one for training, one for evaluation during model tuning (such as identifying a reasonable maximum epoch like here) and, finally, a part that will only be used for validation once all decisions have been made, to assess the actual generalisation performance of the final model. Here, we are

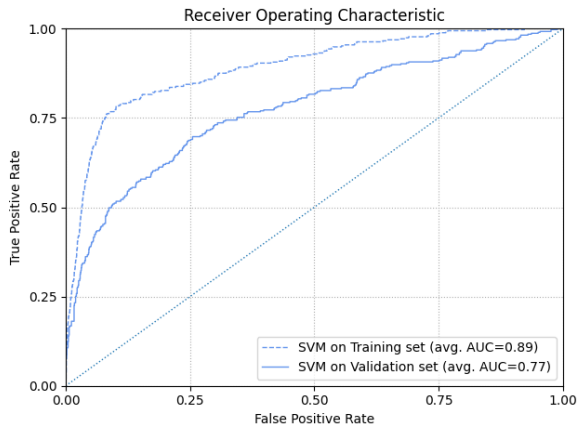

(a) SVM classifier.

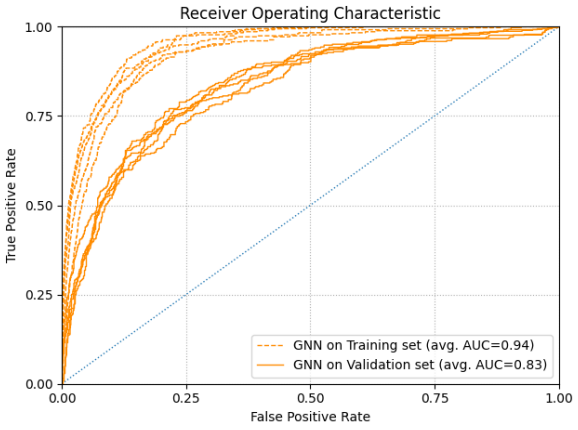

(b) GNN classifier, 5 repeats.

Figure 5.2: ROC Curves for SVM and GNN classifiers trained on AlzPathwayReorg and evaluated on the same dataset (*training set*, dashed line) or on PDMap (*testing set*, solid line).

technically still in the first stage. In the future, potentially, once a single, promising model has been identified and all decisions have been made, there must be anothe validation on completely unseen data.

As a first sanity check for the GNN approach, we verify whether the optimisation procedure is able to overfit the model on the training data. Indeed, the overall loss value converges to a stable minimum and the AUC score for evaluation on the training set at the last epoch is 0.989, indicating a near-perfect fit (not shown in figures).

The initialisation of neural network weights before the training depend on random values. To check whether our training procedure is robust w.r.t.random initialisation, we repeat each run several times with different seed values for the random number generators. Since this seems to be fairly stable, we omit this in future experiments for sake of simplicity.

For both evaluation on PDMap and on ReconMap , the GNN's ROC curve dominates the SVM's curve. This means that for a given FPR deemed acceptable, the GNN model will provide a higher ratio of True Positives. This advantage grows as the decision threshold is lowered, i.e. the GNN model is better particularly when we aim to identify more than just the high-confidence examples. The difference between ROC curves is only slight on evaluation on PDMap but strong on evaluation on ReconMap . This may be due to a better ability of the GNN model to generalise, given different characterstics of ReconMap .

Note how, for both PDMap and ReconMap as evaluation datasets, the validation loss reaches its minimum after just a handful of training epochs. We additionally ran the same experiment with a decreased learning rate ($0.01 \rightarrow 0.001$). There, we can see a smoother decrease the loss value, but also note that the overall achieved minimum is worse than in case of a greater learning rate (see Figure 5.7). This makes it very questionable, how robust model training actually is in this case if the same progress cannot be reliable replicated in a greater number of smaller steps.

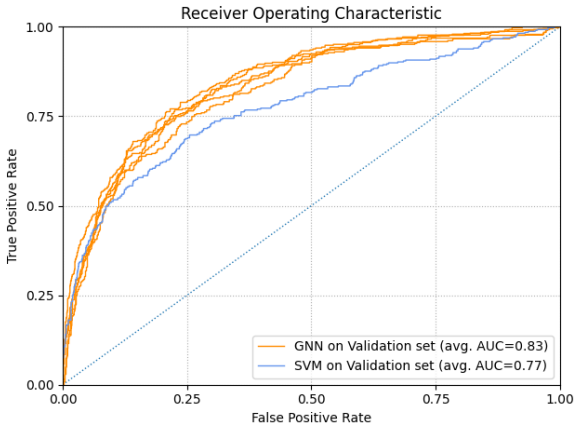

(a) Comparison of ROC Curves of SVM and GNN classifiers.

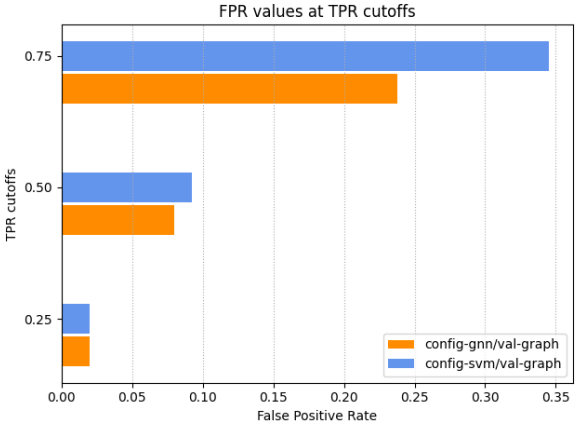

(b) Comparison of FPR values at specific TPR cutoff values (lower is better). These values are specific points from the ROC curve.

Figure 5.3: Direct comparison of SVM and GNN classifier. The data corresponds to the solid lines in Figure 5.2.

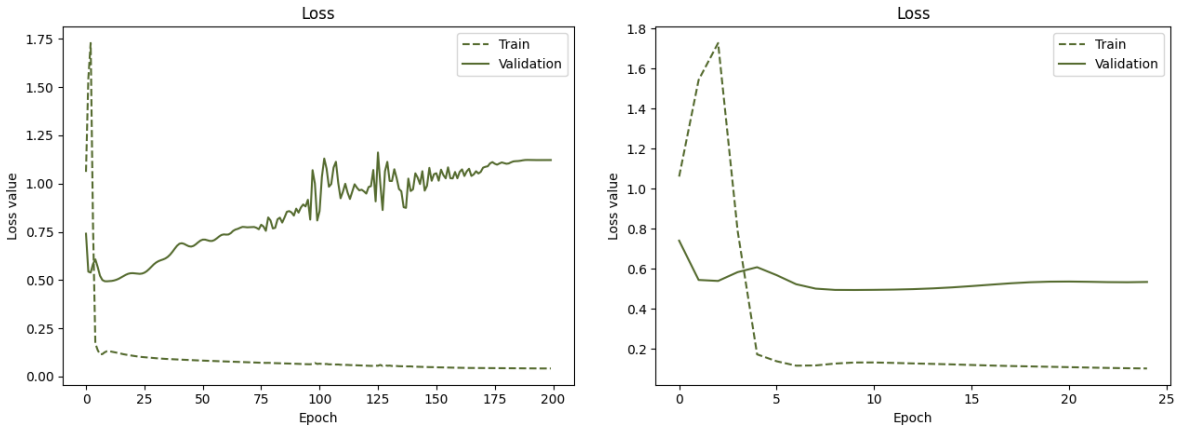

Figure 5.4: Total loss value at each training epoch of the GNN model. The right-hand-side plot a focussed view on the same data.

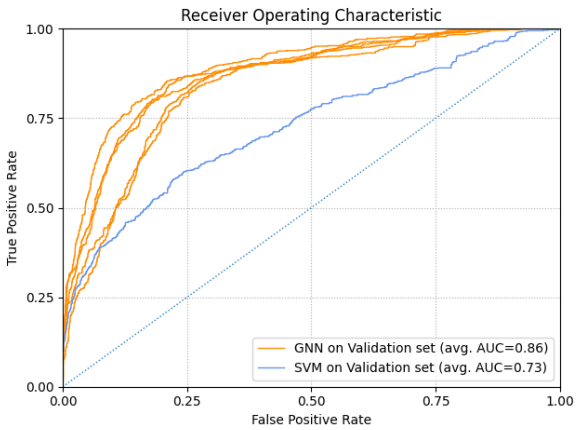

(a) Comparison of ROC Curves of SVM and GNN classifiers.

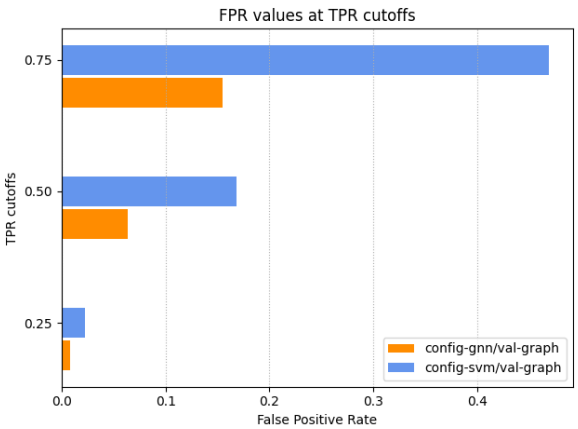

(b) Comparison of FPR values at specific TPR cutoff values (lower is better). These values are specific points from the ROC curve.

Figure 5.5: (AlzPathwayReorg → ReconMap). Direct comparison of SVM and GNN classifier evaluated on ReconMap . The data corresponds to the solid lines in Figure 5.2.

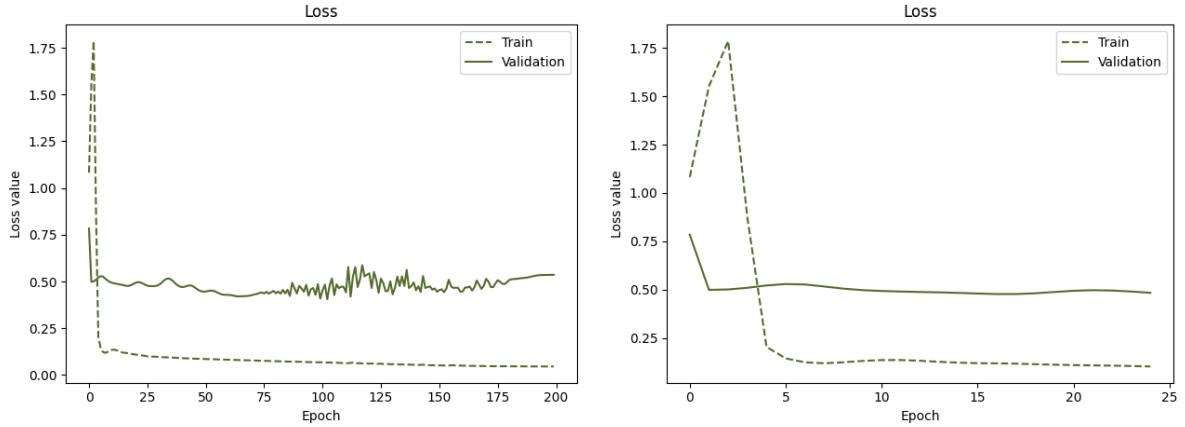

Figure 5.6: Total loss value at each training epoch of the GNN model, evaluted on ReconMap . The right-hand-side plot a focussed view on the same data.

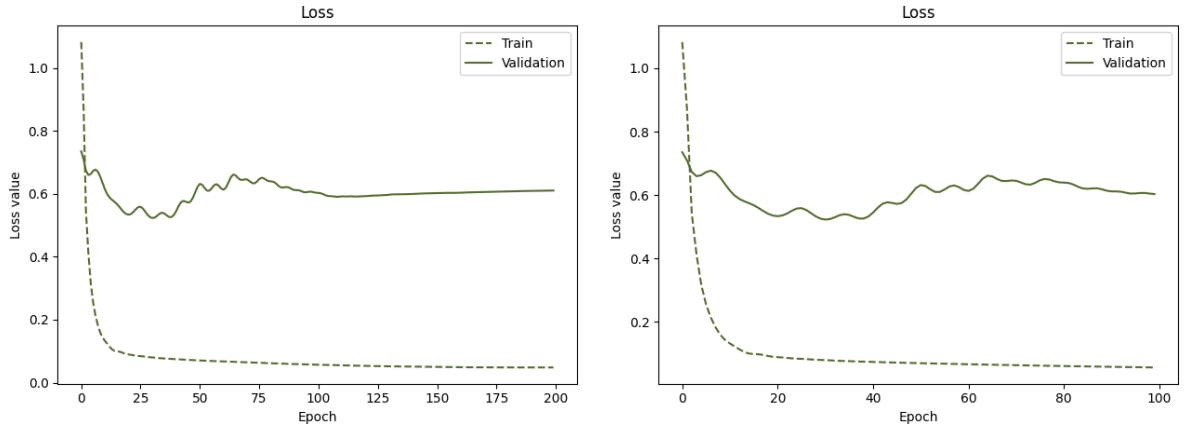

Figure 5.7: Total loss development with decreased learning rate. The plot shows the total loss value at each training epoch of the GNN model, evaluated on ReconMap . The right-hand-side plot a focussed view on the same data.

5.4 Importance of Reorganisation Steps

Motivation Recall that in case of Alzheimer's Disease Map, we are given a sequence of reorganisation steps. The original approach of Nielsen et al.was train a model on the entire sequence of reorganisation steps s.t. the model would mimic the actions of a human curator as closely as possible. They would then evaluate the model on *collapsed* versions of other disease maps. A fully collapsed map potentially has vastly different characteristics than a partially curated map. For instance, a collapsed map is likely to contain species aliases of very high degree (maybe those that appeared often as independent aliases before collapse). In a reorganisation step, on the other hand, the map will already be in part curated and some nodes already duplicated. So, we might effectively be training our models to do one task while testing them on a slightly different task. This consideration is also relevant if we consider a slightly different use-case: one of the first steps in the construction of a disease map may be the semi-automatic concatenation of different pathways, during which species appearing in several pathways will be mapped to the same species alias, i.e. there will be exactly one alias per species. Such a map will very closely resemble a collapsed map in the sense we construct it here. Additionally, a reorganisation sequence is likely to contain contradictory examples: An alias that is duplicated only in a later step will appear as negative example in all previous steps. Further, the concatenation of all reorganisation steps into one big, disconnected graph for training will further amplify the inherent class imbalance. Thus, we deem it interesting to explore how a model will perform if trained not on the reorganisation steps but simply the collapsed version of the final map. This has the additional advantage that in practise, reorganisation steps will rarely be available. The collapsed version, however, can be constructed from any published disease map.

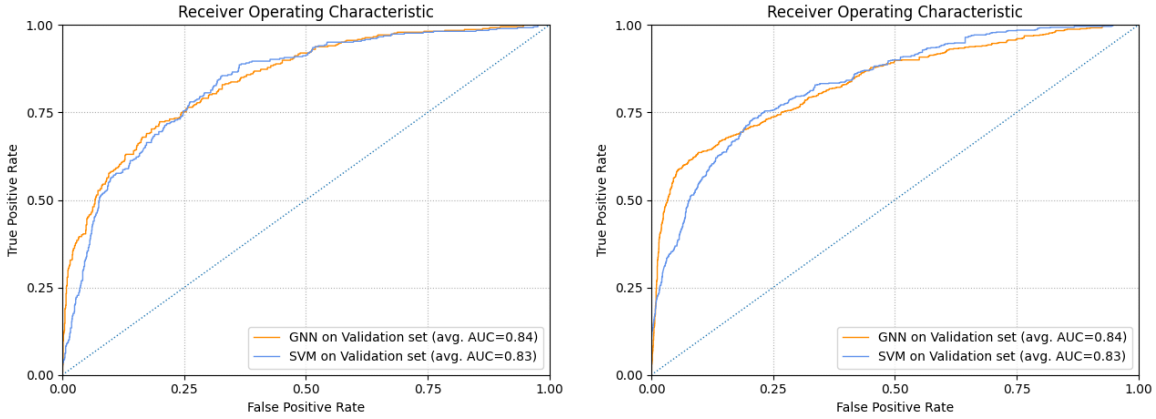

(a) (AlzPathwayLast → PDMap)

(b) (AlzPathwayLast → ReconMap)

Figure 5.8: ROC curves of models trained on collapsed version of the *AlzPathway* map (not the reorganisation steps).

Results & Discussion The results are illustrated in Figure 5.8. Note how both SVM and GNN models do not degrade noticeably in performance (compare to figure Figure **??**). In fact, the SVM model performs *better* when trained on the collapsed map, potentially due to fewer contradictory examples. The GNN models show similar performance.

Another factor to consider here is that collapsed maps are constructed programmatically. When dealing with human-created reorganisation steps, it may be the case that there will be events that may intuitively be interpreted as duplication events but are not picked correctly up by our inferral of ground-truth labels. This is another advantage of the approach of considering only the collapsed version.

Another factor may be that reorganisation steps really are completely independent, as such considering the steps vs the collapsed map would not provide any advantages.

5.5 Handling unbalanced classes

As can be seen from Figure 5.1, we can expect to deal with unbalanced data. A possible concern is that the model may become biased towards predicting the majority class during training since it is simply more likely to occur when evaluating the overall loss.

We consider two simple ways to approach this problem. One is to modify the training data such that it is balanced. Another is to instruct the classifier to give more importance to examples from the minority class.

Undersampling The dataset can be made balanced either by *oversampling* the minory class (coming up with new examples for the minority class) or by *undersampling* the majority class (dropping examples from the majority class) of the majority class from the training data. For oversampling, one may simply duplicate existing examples, or generate synthetic new examples in a more advanced manner (see Section **??**). Although undersampling will decrease the size of the dataset even further, we stick to this approach for sake of simplicity. We undersample the majority class by considering only a random subset for prediction. Note that excluded nodes are not removed from the graph (see Section **??**). We undersample the majority class to contain the same number of examples as the minority class.

Weights If a high weight is specified, misclassifications of positive examples will be penalised more heavily than misclassificaitions of negative examples. In case of neural networks, we can introduce an additional coefficient to the loss function that will determine the weight of prediction outcome of the positive class. We consider the *Weighted Binary Cross Entropy* loss as an extension of **??**, given by

$$\mathcal{L}_{\text{BCE weighted}} = {}^{1}/_{n} \sum_{i=1}^{n} w_i y_i \log(\pi_i) + (1 - y_i) \log(1 - \pi_i) \tag{5.1}$$

We set the weight of the minority class to ${}^{n_{\text{maj}}}/_{n_{\text{min}}}$ where n_{maj} is the number of examples in the majority class and n_{min} the number of examples in the minority class. In other words, if every example is counted according to its weight, the class counts are balanced.

Results & Discussion Experimental results show that neither undersampling nor custom class weights have substantial effect on model performance (AlzPathwayLast → PDMap : GNN-AUC= 0.83; SVM-AUC= 0.83). We omit visualisations here due to space constraints. For sake of simplicity, we omit undersampling or weights in future experiments.

5.6 Importance of Message-Passing

We explore whether the message-passing layers of the GNN model actually provide an advantage over a neural network consisting simply of fully-connected layers. Further, we aim to compare which graph structure serves better for message-passing: We can interpret the given bipartite graph of species aliases and reactions as a simple graph, or we can consider its bipartite projection (as in previous experiments).

To assess the importance of using message-passing layers at all, we compare to a model that has the message-passing layers replaced with fully-connected layers.

Note that for message-passing on the simple graph interpretation, of the structural features described in TODO, we can only consider those computed on the simple graph.

Results are summarised in Figure **??**. It is evident that on this dataset, using these features *, message-passing does not provide a big advantage in overall performance.

* We will consider a different feature set in TODO.

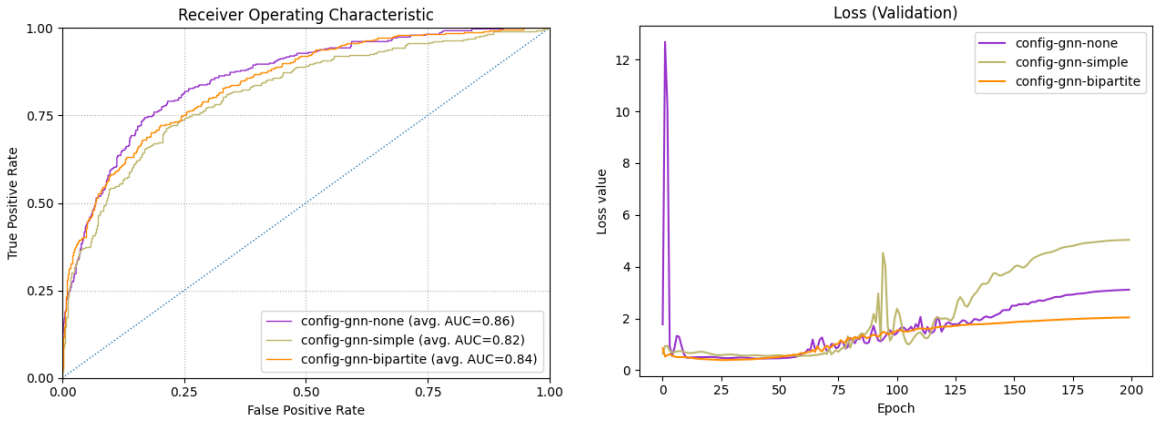

(a) ...

(b) Validation loss per training epoch for different model variants.

Figure 5.9: (AlzPathwayLast → PDMap) Comparison of performance of NN models with and without message-passing layers. `config-gnn-none` has fully-connected layers instead of message-passing layers. `config-gnn-bipartite` is the same model as considered in previous experiments.

However, note that loss curves look different TODO.

Further, the results on the graph interpretation are probably not meaningful since the message-passing itself does not make a real difference.

5.7 Attention Mechanism

5.8 Feature Selection

5.9 Gene Ontology Annotations

5.10 Additional Training Data

...

5.11 Attachment of Edges

We provide some examples for successful and problematic cases in Figure **??**. From manual inspection, the vast majority of results seemed to be reasonable clusterings, and in rare cases, ambiguous situations like illustrated here occured.

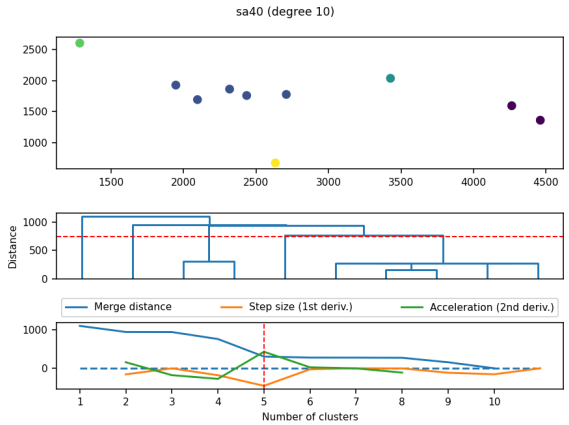

(a) Example for which the heuristic yields an intuitive clustering. Note that outliers do not distort the clustering result and are assigned their own cluster.

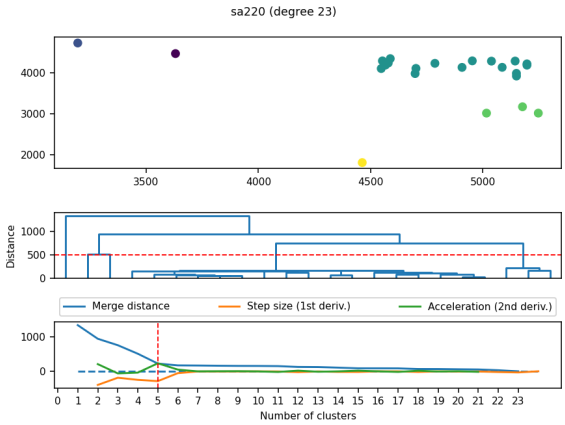

(b) Example in which using the second derivative yields a clustering that intuitively seems more reasonable. The first derivative has its minimum at 2 clusters.

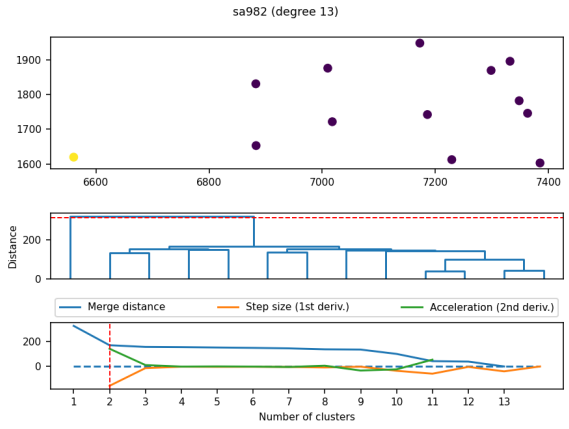

(c) Distances between the purple points are not much different from the distance between the yellow point and the purple cluster (measured by *single linkage*). While the heuristic yields only two clusters, it may have also been feasible to create many clusters. Indeed, the second derivative curve shows another local maximum at 11 clusters.

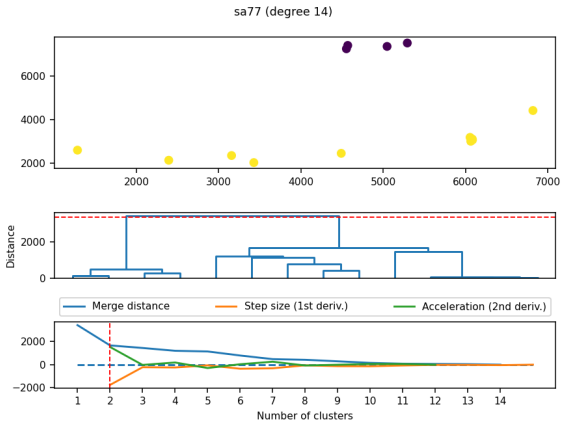

(d) Another example where large intra-cluster variance is problematic. Contrary to the heuristic's output, it may be preferrable to further split the yellow cluster.

Figure 5.10: Examples for the clustering procedure described in Section **??**. The topmost scatterplot shows the positions of neighbours of a given node in the layout (given node and edges are not shown). Below, a clustering dendrogram describes the distances between two any clusters as they were merged. Finally, the sequence of merge distances as well as its first and second derivative. Taking the minumum, resp. maximum yields a hint for the number of clusters to choose. The red line indicates the suggested choice for the number of clusters and thus a concrete clustering, determing the merge node in the dendrogram where the "cut" should be made. All examples are from AlzPathwayReorg .

6 Discussion

7 Outlook & Future Work

Appendix

.1 Notation & Abbreviations

- Vectors and matrices are usually set in bold letters, e.g. $\mathbf{x}$ or $\mathbf{A}$. Vectors are assumed to column vectors unless otherwise specified. $\cdot^T$ denotes the transpose.
- $\|\cdot\|$ denotes the l_2-norm, or set cardinality.
- G commonly denotes a graph, $V(G)$ is its vertex set and $E(G)$ its edge set. Whether we consider a directed, undirected, bipartite or simple graph will be made clear from context.
- $\mathcal{N}(v)$ denotes the graph neighbourhood of node v. Unless otherwise specified, this is the direct 1-hop neighbourhood.
- The *bipartite projection* of a bipartite graph with node set $V = A \cup B$ that is the disjoint union of species aliases A and reactions B, the *bipartite projection onto* A is the simple graph with node set A in which $v_i, v_j \in A$ are connected if and only if in the bipartite they have a common neighbour in B.
- A *species* is an actor in a biological system. Examples for species are proteins, smaller molecules, but also drugs or phenotypes. A *species alias* is a visual representation of a species in a drawing. There can be multiple species aliases corresponding to the same species. A *complex species alias* represents a collection of species aliases, commonly representing protein complexes.

.2 Acknowledgements

References

[1] Camilo Ruiz, Marinka Zitnik, and Jure Leskovec. 'Identification of Disease Treatment Mechanisms through the Multiscale Interactome'. In: *Nature Communications* 12.1 (1 Mar. 19, 2021), p. 1796. DOI: 10.1038/s41467-021-21770-8. (Visited on 03/22/2021) (cited on page 2).

[2] Albert-László Barabási, Natali Gulbahce, and Joseph Loscalzo. 'Network Medicine: A Network-Based Approach to Human Disease'. In: *Nature Reviews Genetics* 12.1 (1 Jan. 2011), pp. 56–68. DOI: 10.1038/nrg2918. (Visited on 10/04/2021) (cited on page 2).

[3] Marek Ostaszewski et al. 'Community-Driven Roadmap for Integrated Disease Maps'. In: *Briefings in Bioinformatics* 20.2 (Mar. 25, 2019), pp. 659–670. DOI: 10.1093/bib/bby024. (Visited on 06/08/2021) (cited on page 2).

[4] Alexander Mazein et al. 'Systems Medicine Disease Maps: Community-Driven Comprehensive Representation of Disease Mechanisms'. In: *NPJ systems biology and applications* 4 (2018), p. 21. DOI: 10.1038/s41540-018-0059-y (cited on page 2).

[5] Donna Maglott et al. 'Entrez Gene: Gene-Centered Information at NCBI'. In: *Nucleic Acids Research* 33 (Database issue Jan. 1, 2005), pp. D54–58. DOI: 10.1093/nar/gki031 (cited on pages 3, 5).

[6] The UniProt Consortium. 'UniProt: The Universal Protein Knowledgebase in 2021'. In: *Nucleic Acids Research* 49.D1 (Jan. 8, 2021), pp. D480–D489. DOI: 10.1093/nar/gkaa1100. (Visited on 10/04/2021) (cited on pages 3, 5).

[7] Kazuhiro A. Fujita et al. 'Integrating Pathways of Parkinson's Disease in a Molecular Interaction Map'. In: *Molecular Neurobiology* 49.1 (Feb. 1, 2014), pp. 88–102. DOI: 10.1007/s12035-013-8489-4. (Visited on 06/14/2021) (cited on pages 4, 16, 25).

[8] Romain Bourqui et al. 'Metabolic Network Visualization Eliminating Node Redundance and Preserving Metabolic Pathways'. In: *BMC Systems Biology* 1.1 (July 3, 2007), p. 29. DOI: 10.1186/1752-0509-1-29. (Visited on 09/23/2021) (cited on page 4).

[9] Martin Siebenhaller et al. 'Human-like Layout Algorithms for Signalling Hypergraphs: Outlining Requirements'. In: *Briefings in Bioinformatics* 21.1 (Jan. 17, 2020), pp. 62–72. DOI: 10.1093/bib/bby099. (Visited on 06/08/2021) (cited on page 4).

[10] Hsiang-Yun Wu et al. 'Metabopolis: Scalable Network Layout for Biological Pathway Diagrams in Urban Map Style'. In: *BMC Bioinformatics* 20.1 (Apr. 15, 2019), p. 187. DOI: 10.1186/s12859-019-2779-4. (Visited on 09/23/2021) (cited on page 4).

[11] David S. Wishart et al. 'DrugBank: A Knowledgebase for Drugs, Drug Actions and Drug Targets'. In: *Nucleic Acids Research* 36 (suppl_1 Jan. 1, 2008), pp. D901–D906. DOI: 10.1093/nar/gkm958. (Visited on 10/05/2021) (cited on page 5).

[12] Michael Ashburner et al. 'Gene Ontology: Tool for the Unification of Biology'. In: *Nature Genetics* 25.1 (1 May 2000), pp. 25–29. DOI: 10.1038/75556. (Visited on 10/05/2021) (cited on page 6).

[13] Vladimir Vapnik. 'Principles of Risk Minimization for Learning Theory'. In: (), p. 8 (cited on page 6).

[14] Michael M. Bronstein et al. *Geometric Deep Learning: Grids, Groups, Graphs, Geodesics, and Gauges*. May 2, 2021. URL: http://arxiv.org/abs/2104.13478 (visited on 05/06/2021) (cited on page 6).

[15] Aston Zhang et al. 'Dive into Deep Learning'. In: (), p. 1021 (cited on pages 6, 7, 9).

[16] Lex Flagel, Yaniv Brandvain, and Daniel R. Schrider. 'The Unreasonable Effectiveness of Convolutional Neural Networks in Population Genetic Inference'. In: *Molecular Biology and Evolution* 36.2 (Feb. 1, 2019), pp. 220–238. DOI: 10.1093/molbev/msy224 (cited on page 7).

[17] Genta Aoki and Yasubumi Sakakibara. 'Convolutional Neural Networks for Classification of Alignments of Non-Coding RNA Sequences'. In: *Bioinformatics* 34.13 (July 1, 2018), pp. i237–i244. DOI: 10.1093/bioinformatics/bty228. (Visited on 10/06/2021) (cited on page 7).

[18] William L. Hamilton, Rex Ying, and Jure Leskovec. *Inductive Representation Learning on Large Graphs*. Sept. 10, 2018. URL: http://arxiv.org/abs/1706.02216 (visited on 06/16/2021) (cited on page 8).

[19] Rex Ying et al. *Hierarchical Graph Representation Learning with Differentiable Pooling*. Feb. 20, 2019. URL: http://arxiv.org/abs/1806.08804 (visited on 02/04/2021) (cited on page 8).

[20] Thomas N. Kipf and Max Welling. *Semi-Supervised Classification with Graph Convolutional Networks*. Feb. 22, 2017. URL: http://arxiv.org/abs/1609.02907 (visited on 12/07/2020) (cited on page 8).

[21] Petar Veličković et al. *Graph Attention Networks*. Feb. 4, 2018. URL: http://arxiv.org/abs/1710.10903 (visited on 01/05/2021) (cited on page 8).

[22] Ashish Vaswani et al. *Attention Is All You Need*. Dec. 5, 2017. URL: http://arxiv.org/abs/1706.03762 (visited on 10/10/2021) (cited on page 9).

[23] Taocheng Liu, Xiangbin Ye, and Bei Sun. 'Combining Convolutional Neural Network and Support Vector Machine for Gait-Based Gender Recognition'. In: *2018 Chinese Automation Congress (CAC)*. 2018 Chinese Automation Congress (CAC). Nov. 2018, pp. 3477–3481. DOI: 10.1109/CAC.2018.8623118 (cited on page 9).

[24] Sami Tibshirani, Harry Friedman, and Trevor Hastie. 'The Elements of Statistical Learning'. In: (2017), p. 764 (cited on page 10).

[25] Sune S. Nielsen et al. 'Machine Learning to Support the Presentation of Complex Pathway Graphs'. In: *IEEE/ACM Transactions on Computational Biology and Bioinformatics* (2019), pp. 1–1. DOI: 10.1109/TCBB.2019.2938501 (cited on pages 13–15, 18–21, 25, 26, 30).

[26] Akira Funahashi et al. 'CellDesigner 3.5: A Versatile Modeling Tool for Biochemical Networks'. In: *Proceedings of the IEEE* 96.8 (Aug. 2008), pp. 1254–1265. DOI: 10.1109/JPROC.2008.925458 (cited on page 14).

[27] Piotr Gawron et al. 'MINERVA—a Platform for Visualization and Curation of Molecular Interaction Networks'. In: *npj Systems Biology and Applications* 2.1 (1 Sept. 22, 2016), pp. 1–6. DOI: 10.1038/npjsba.2016.20. (Visited on 10/04/2021) (cited on page 14).

[28] Paul Shannon et al. 'Cytoscape: A Software Environment for Integrated Models of Biomolecular Interaction Networks'. In: *Genome Research* 13.11 (Jan. 11, 2003), pp. 2498–2504. DOI: 10.1101/gr.1239303. (Visited on 05/04/2021) (cited on page 14).

[29] Hendrik Rohn et al. 'VANTED v2: A Framework for Systems Biology Applications'. In: *BMC Systems Biology* 6.1 (2012), p. 139. DOI: 10.1186/1752-0509-6-139. (Visited on 04/24/2019) (cited on page 14).

[30] Mikael Huss and Petter Holme. 'Currency and Commodity Metabolites: Their Identification and Relation to the Modularity of Metabolic Networks'. In: *IET Systems Biology* 1.5 (Sept. 1, 2007), pp. 280–285. DOI: 10.1049/iet-syb:20060077. (Visited on 06/09/2021) (cited on pages 14, 15).

[31] Eun-Youn Kim, Daniel Ashlock, and Sung Ho Yoon. 'Identification of Critical Connectors in the Directed Reaction-Centric Graphs of Microbial Metabolic Networks'. In: *BMC bioinformatics* 20.1 (June 13, 2019), p. 328. DOI: 10.1186/s12859-019-2897-z (cited on page 14).

[32] Annegret Liebers. 'Planarizing Graphs — A Survey and Annotated Bibliography'. In: (2001), p. 74 (cited on page 14).

[33] Faisal N. Abu-Khzam et al. 'Cluster Editing with Vertex Splitting'. In: *Combinatorial Optimization*. Ed. by Jon Lee, Giovanni Rinaldi, and A. Ridha Mahjoub. Vol. 10856. Lecture Notes in Computer Science. Cham: Springer International Publishing, 2018, pp. 1–13. DOI: 10.1007/978-3-319-96151-4_1. (Visited on 10/13/2021) (cited on page 14).

[34] P. Eades and C. F. X. de Mendonça N. 'Vertex Splitting and Tension-Free Layout'. In: *Graph Drawing*. Ed. by Franz J. Brandenburg. Red. by G. Goos, J. Hartmanis, and J. van Leeuwen. Vol. 1027. Lecture Notes in Computer Science. Berlin, Heidelberg: Springer Berlin Heidelberg, 1996, pp. 202–211. DOI: 10.1007/BFb0021804. (Visited on 06/16/2021) (cited on page 14).

[35] Tomihisa Kamada and Satoru Kawai. 'An Algorithm for Drawing General Undirected Graphs'. In: *Information Processing Letters* 31.1 (1989), p. 9 (cited on page 14).

[36] J. Li. *Eliminate Wire Crossings by Node Duplication*. 2008. URL: https://www.semanticscholar.org/paper/Eliminate-Wire-Crossings-by-Node-Duplication-Li/f15e6d3a207ca83339ee1901047a6d7905cc4d39 (visited on 09/23/2021) (cited on page 14).

[37] Doo-Kwon Paik, S. Reddy, and S. Sahni. 'Vertex Splitting in Dags and Applications to Partial Scan Designs and Lossy Circuits'. In: *Int. J. Found. Comput. Sci.* (1998). DOI: 10.1142/S0129054198000301 (cited on page 14).

[38] M. Mayer and F. Erçal. 'Genetic Algorithms for Vertex Splitting in DAGs'. In: *undefined* (1993). (Visited on 10/13/2021) (cited on page 14).

[39] N. Henr, A. Bezerianos, and J.-D. Fekete. 'Improving the Readability of Clustered Social Networks Using Node Duplication'. In: *IEEE Transactions on Visualization and Computer Graphics* 14.6 (Nov. 2008), pp. 1317–1324. DOI: 10.1109/TVCG.2008.141. (Visited on 06/08/2021) (cited on page 14).

[40] Ichcha Manipur et al. 'Clustering Analysis of Tumor Metabolic Networks'. In: *BMC Bioinformatics* 21.10 (Aug. 25, 2020), p. 349. DOI: 10.1186/s12859-020-03564-9. (Visited on 01/06/2021) (cited on page 15).

[41] H. Ma and A. Zeng. 'Reconstruction of Metabolic Networks from Genome Data and Analysis of Their Global Structure for Various Organisms'. In: *undefined* (2003). (Visited on 05/28/2021) (cited on page 15).

[42] S. Schuster et al. 'Exploring the Pathway Structure of Metabolism: Decomposition into Subnetworks and Application to Mycoplasma Pneumoniae'. In: *Bioinformatics* 18.2 (Feb. 1, 2002), pp. 351–361. DOI: 10.1093/bioinformatics/18.2.351. (Visited on 11/20/2020) (cited on page 15).

[43] M. E. J. Newman. 'Modularity and Community Structure in Networks'. In: *Proceedings of the National Academy of Sciences* 103.23 (June 6, 2006), pp. 8577–8582. DOI: 10.1073/pnas.0601602103. (Visited on 04/12/2019) (cited on page 15).

[44] Roger Guimerà and Luís A. Nunes Amaral. 'Functional Cartography of Complex Metabolic Networks'. In: *Nature* 433.7028 (7028 Feb. 2005), pp. 895–900. DOI: 10.1038/nature03288. (Visited on 06/09/2021) (cited on page 15).

[45] Markus Rohrschneider et al. 'A Novel Grid-Based Visualization Approach for Metabolic Networks with Advanced Focus&Context View'. In: *Graph Drawing*. Ed. by David Eppstein and Emden R. Gansner. Red. by David Hutchison et al. Vol. 5849. Lecture Notes in Computer Science. Berlin, Heidelberg: Springer Berlin Heidelberg, 2010, pp. 268–279. DOI: 10.1007/978-3-642-11805-0_26. (Visited on 06/11/2021) (cited on page 15).

[46] G. Joshi-Tope et al. 'Reactome: A Knowledgebase of Biological Pathways'. In: *Nucleic Acids Research* 33 (suppl_1 Jan. 1, 2005), pp. D428–D432. DOI: 10.1093/nar/gki072. (Visited on 10/13/2021) (cited on page 15).

[47] Alice C. Villéger, Stephen R. Pettifer, and Douglas B. Kell. 'Arcadia: A Visualization Tool for Metabolic Pathways'. In: *Bioinformatics* 26.11 (June 1, 2010), pp. 1470–1471. DOI: 10.1093/bioinformatics/btq154. (Visited on 10/04/2021) (cited on page 15).

[48] Peter Droste, Katharina Nöh, and Wolfgang Wiechert. 'Omix - A Visualization Tool for Metabolic Networks with Highest Usability and Customizability in Focus'. In: *Chemie Ingenieur Technik* 85.6 (June 2013), pp. 849–862. DOI: 10.1002/cite.201200234. (Visited on 10/04/2021) (cited on page 15).

[49] Soichi Ogishima et al. 'AlzPathway, an Updated Map of Curated Signaling Pathways: Towards Deciphering Alzheimer's Disease Pathogenesis'. In: *Methods in Molecular Biology (Clifton, N.J.)* 1303 (2016), pp. 423–432. DOI: 10.1007/978-1-4939-2627-5_25 (cited on pages 16, 25).

[50] Marek Ostaszewski et al. 'COVID-19 Disease Map, Building a Computational Repository of SARS-CoV-2 Virus-Host Interaction Mechanisms'. In: *Scientific Data* 7.1 (May 5, 2020), p. 136. DOI: 10.1038/s41597-020-0477-8 (cited on page 16).

[51] Satoshi Mizuno et al. 'Network Analysis of a Comprehensive Knowledge Repository Reveals a Dual Role for Ceramide in Alzheimer's Disease'. In: *PloS One* 11.2 (2016), e0148431. DOI: 10.1371/journal.pone.0148431 (cited on pages 16, 25).

[52] Nicolas Sompairac et al. 'Metabolic and Signalling Network Maps Integration: Application to Cross-Talk Studies and Omics Data Analysis in Cancer'. In: *BMC Bioinformatics* 20 (Suppl 4 Apr. 18, 2019). DOI: 10.1186/s12859-019-2682-z. (Visited on 04/14/2021) (cited on page 16).

[53] Matteo Tiezzi, Gabriele Ciravegna, and Marco Gori. *Graph Neural Networks for Graph Drawing*. Sept. 21, 2021. URL: http://arxiv.org/abs/2109.10061 (visited on 10/13/2021) (cited on page 16).

[54] Emden R. Gansner, Yehuda Koren, and Stephen North. 'Graph Drawing by Stress Majorization'. In: *Graph Drawing*. Ed. by János Pach. Red. by David Hutchison et al. Vol. 3383. Lecture Notes in Computer Science. Berlin, Heidelberg: Springer Berlin Heidelberg, 2005, pp. 239–250. DOI: 10.1007/978-3-540-31843-9_25. (Visited on 03/31/2020) (cited on page 16).

[55] Ronghui You et al. 'DeepGraphGO: Graph Neural Network for Large-Scale, Multispecies Protein Function Prediction'. In: *Bioinformatics* 37 (Supplement_1 July 1, 2021), pp. i262–i271. DOI: 10.1093/bioinformatics/btab270. (Visited on 10/13/2021) (cited on page 16).

[56] Xiaoshi Zhong, Rama Kaalia, and Jagath C. Rajapakse. 'GO2Vec: Transforming GO Terms and Proteins to Vector Representations via Graph Embeddings'. In: *BMC Genomics* 20.9 (Feb. 18, 2020), p. 918. DOI: 10.1186/s12864-019-6272-2. (Visited on 09/06/2021) (cited on pages 16, 22).

[57] Neal Ravindra et al. 'Disease State Prediction from Single-Cell Data Using Graph Attention Networks'. In: *Proceedings of the ACM Conference on Health, Inference, and Learning*. CHIL '20. New York, NY, USA: Association for Computing Machinery, Apr. 2, 2020, pp. 121–130. DOI: 10.1145/3368555.3384449. (Visited on 04/21/2021) (cited on page 16).

[58] Jonathan M. Stokes et al. 'A Deep Learning Approach to Antibiotic Discovery'. In: *Cell* 180.4 (Feb. 2020), 688–702.e13. DOI: 10.1016/j.cell.2020.01.021. (Visited on 10/14/2021) (cited on page 17).

[59] David Duvenaud et al. *Convolutional Networks on Graphs for Learning Molecular Fingerprints*. Nov. 3, 2015. URL: http://arxiv.org/abs/1509.09292 (visited on 01/21/2021) (cited on page 17).

[60] Oliver Wieder et al. 'A Compact Review of Molecular Property Prediction with Graph Neural Networks'. In: *Drug Discovery Today: Technologies* (Dec. 17, 2020). DOI: 10.1016/j.ddtec.2020.11.009. (Visited on 10/14/2021) (cited on page 17).

[61] Thomas Gaudelet et al. *Utilising Graph Machine Learning within Drug Discovery and Development*. Dec. 9, 2020. URL: http://arxiv.org/abs/2012.05716 (visited on 01/14/2021) (cited on page 17).

[62] Mayank Baranwal et al. 'A Deep Learning Architecture for Metabolic Pathway Prediction'. In: *Bioinformatics (Oxford, England)* 36.8 (Apr. 15, 2020), pp. 2547–2553. DOI: 10.1093/bioinformatics/btz954 (cited on page 17).

[63] Bajaj, Heereguppe, and Sumath. *Graph Convolutional Networks to Explore Drug and Disease Relationships in Biological Networks*. 2017. (Visited on 10/14/2021) (cited on page 17).

[64] Marinka Zitnik, Monica Agrawal, and Jure Leskovec. 'Modeling Polypharmacy Side Effects with Graph Convolutional Networks'. In: *Bioinformatics* 34.13 (July 1, 2018), pp. i457–i466. DOI: 10.1093/bioinformatics/bty294. (Visited on 12/14/2020) (cited on page 17).

[65] Hryhorii Chereda et al. 'Explaining Decisions of Graph Convolutional Neural Networks: Patient-Specific Molecular Subnetworks Responsible for Metastasis Prediction in Breast Cancer'. In: *Genome Medicine* 13 (Mar. 11, 2021), p. 42. DOI: 10.1186/s13073-021-00845-7. (Visited on 10/14/2021) (cited on page 17).

[66] Xiao-Meng Zhang et al. 'Graph Neural Networks and Their Current Applications in Bioinformatics'. In: *Frontiers in Genetics* 12 (July 29, 2021), p. 690049. DOI: 10.3389/fgene.2021.690049. (Visited on 10/14/2021) (cited on page 17).

[67] Vincent Henry et al. 'Converting Disease Maps into Heavyweight Ontologies: General Methodology and Application to Alzheimer's Disease'. In: *Database: The Journal of Biological Databases and Curation* 2021 (Feb. 16, 2021), baab004. DOI: 10.1093/database/baab004 (cited on page 17).

[68] Marek Ostaszewski et al. 'Clustering Approaches for Visual Knowledge Exploration in Molecular Interaction Networks'. In: *BMC Bioinformatics* 19.1 (Aug. 29, 2018), p. 308. DOI: 10.1186/s12859-018-2314-z. (Visited on 06/07/2021) (cited on pages 17, 23).

[69] *CellDesigner 4 Extension Tag Specification Document*. 2010. URL: http://www.celldesigner.org/documents/CellDesigner4ExtensionTagSpecificationE.pdf (visited on 08/16/2021) (cited on page 18).

[70] Ulrik Brandes and Thomas Erlebach, eds. *Network Analysis: Methodological Foundations*. LCNS, Tutorial 3418. Berlin ; New York: Springer, 2005. 471 pp. (cited on page 20).

[71] Satoshi Mizuno et al. 'AlzPathway: A Comprehensive Map of Signaling Pathways of Alzheimer's Disease'. In: *BMC Systems Biology* 6.1 (May 30, 2012), p. 52. DOI: 10.1186/1752-0509-6-52. (Visited on 06/02/2021) (cited on page 25).

[72] S. Ogishima et al. 'A Map of Alzheimer's Disease-Signaling Pathways: A Hope for Drug Target Discovery'. In: *Clinical Pharmacology and Therapeutics* 93.5 (May 2013), pp. 399–401. DOI: 10.1038/clpt.2013.37 (cited on page 25).

[73] Marek Ostaszewski. *AlzPathway Regorganisation Steps for Increased Modularity*. Zenodo, June 25, 2021. DOI: 10.5281/zenodo.5032278. (Visited on 06/28/2021) (cited on page 25).

[74] Alberto Noronha et al. 'ReconMap: An Interactive Visualization of Human Metabolism'. In: *Bioinformatics* 33.4 (Feb. 15, 2017), pp. 605–607. DOI: 10.1093/bioinformatics/btw667. (Visited on 07/09/2021) (cited on page 25).

[75] Ines Thiele et al. 'A Community-Driven Global Reconstruction of Human Metabolism'. In: *Nature Biotechnology* 31.5 (5 May 2013), pp. 419–425. DOI: 10.1038/nbt.2488. (Visited on 10/18/2021) (cited on page 25).

[76] Jiaxuan You, Rex Ying, and Jure Leskovec. *Design Space for Graph Neural Networks*. Nov. 17, 2020. URL: http://arxiv.org/abs/2011.08843 (visited on 02/26/2021) (cited on page 26).